Title:

S1 hydrophobic residues modulate voltage sensing phosphatase enzymatic function and voltage sensing

Condensed title:

S1 hydrophobic residues modulate voltage sensing

Vamseedhar Rayaprolu [1,4], Heini M. Miettinen [1], William Baker [1], Victoria C. Young [2], Matthew Fisher [1], Gwendolyn Mueller [1], William O. Rankin [1], J. Jack Kelly [1], William J. Ratzan [1,5], Lee Min Leong [3], Joshua A. Davisson [1,6], Bradley J. Baker [3], Susy C. Kohout [2,#].

[1] Montana State University, Department of Cell Biology & Neuroscience, Department of Microbiology & Cell Biology, Bozeman, MT, USA

[2] Cooper Medical School of Rowan University, Dept of Biomedical Sciences, Camden, NJ

[3] Brain Science Institute, Korea Institute of Science & Technology (KIST), Division of Bio-Medical Science & Technology, KIST School, Korea University of Science & Technology (UST), Seoul, South Korea.

Current locations:

[4] Pacific Northwest CryoEM Center, Portland, OR.

[5] Harvard University, Dept. of Systems Biology, Boston, MA.

[6] University of Minnesota, Dept. of Biochemistry, Molecular Biology & Biophysics, Minneapolis, MN.

corresponding author: kohout@rowan.edu

Abstract

The voltage sensing domain (VSD) is a four-helix modular protein domain that converts electrical signals into conformational changes, leading to open pores and active enzymes. In most voltage sensing proteins, the VSDs do not interact with one another and the S1-S3 helices are considered mainly as scaffolding. The two exceptions are the voltage sensing phosphatase (VSP) and the proton channel (Hv). VSP is a voltage-regulated enzyme and Hv's are channels that only have VSDs. To investigate the S1 contribution to VSP function, we individually mutated four hydrophobic amino acids in S1 to alanine (F127, I131, I134 and L137). We also combined these mutations to generate quadruple mutation designated S1-Q. Most of these mutations shifted the voltage dependence of activity to higher voltages though interestingly, not all substrate reactions were the same. The kinetics of enzymatic activity were also altered with some mutations significantly slowing down dephosphorylation. The voltage dependence of VSD motions were consistently shifted to lower voltages and indicated a second voltage dependent motion. Co-immunoprecipitation demonstrated that none of the mutations broke the VSP dimer indicating that the S1 impact could stem from intrasubunit and/or intersubunit interactions. Lastly, when the same alanine mutations were introduced into a genetically encoded voltage indicator, they dramatically altered the optical readings, making some of the kinetics faster and shifting the voltage dependence. These results indicate that the S1 helix in VSP plays a critical role in tuning the enzyme's conformational response to membrane potential transients and influencing the function of the VSD.

Introduction

Voltage sensing domains (VSDs) are well known modular domains that cause proteins to be regulated by changes in membrane potential (1). They are composed of four transmembrane helices, labeled S1-S4, with S4 conferring the voltage dependence of the domain via arginines embedded in the helix. The voltage regulated family of proteins was long thought to be composed solely of channels, but the discovery of the voltage sensing phosphatase (VSP) broadened the

biological role this group of proteins play in cellular physiology. Instead of having channel function, VSP connects a VSD to a phosphatase domain that will dephosphorylate phosphatidylinositol phosphates (PIPs) in a voltage dependent manner (2) (Fig 1A). Several studies show that the VSD from VSP functions in the same way as those from channels with S4 movements propagating to the connected linker (2–4). The VSP linker then propagates the conformational change to the phosphatase domain that then removes both the 3- and 5-phosphates from the PIP inositol ring (2, 5–10) (Fig 1B). The phosphatase domain is composed of a catalytic domain and a membrane binding C2 domain with mutations in either domain impacting catalytic activity (2, 9, 11). In particular, VSP removes the 5-phosphate from phosphatidylinositol-3,4,5-trisphosphate [PI(3,4,5)P_3] to generate phosphatidylinositol-3,4-trisphosphate [PI(3,4)P_2] and from phosphatidylinositol-4,5-trisphosphate [PI(4,5)P_2] to generate phosphatidylinositol-4-trisphosphate PI(4)P. In addition, VSP will remove the 3-phosphate from PI(3,4,5)P_3 to generate PI(4,5)P_2 and from PI(3,4)P_2 to generate PI(4)P. Thus, while VSP catalyzes two types of reactions (3- and 5-phosphate removal), it has three different possible substrates. As a result of being the only enzyme directly coupled to a VSD, VSP serves as a unique member of the family for better understanding how VSD's change conformation in response to changes in the membrane potential.

Because of the importance of S4, many studies have been dedicated to understanding how S4 moves in response to voltage and how it transfers the activation information to the rest of the protein (12, 13). The S2 and S3 helices are known to contain counter charges for the S4 arginines (14, 15). The S1 helix is also known to contribute to the hydrophobic plug (gating pore) that prevents ion conduction through the VSD while still allowing the Arg to move in response to voltage (16). However, S1-S3 is mainly considered a scaffold when investigating voltage dependence (13). In contrast, S1 appears to play a more active role in both the voltage-gated proton channel (Hv) and the voltage sensing phosphatase (VSP). Specifically, S1 may help mediate dimerization in Hv (17–19) and is proposed to play a role in gating Hv's proton conduction because it moves during the

79 opening transition as opposed to S4 which moves before the opening transition (20). In VSP, S1
80 may also help mediate dimerization (21, 22). Importantly, others have shown a functional impact of
81 S1 where amino acid 126 in the *Ciona intestinalis* VSP (Ci-VSP) S1 tunes voltage sensing over 2
82 orders of magnitude (23). Mutations in S1 also shift enzyme activity in Ci-VSP (24), and in *Danio*
83 *rerio* VSP (Dr-VSP) (25). In addition, the S1 in Ci-VSP appears to move in response to voltage
84 sensing when the phosphatase is removed (26). A complete picture of how S1 influences enzyme
85 activation and voltage sensing in VSP remains unclear. Here, we investigate how VSP uses S1 to
86 control and modulate enzyme activity and the VSD.
87
88 The discovery of VSP also boosted our understanding of the modularity of the VSD and has led to
89 the generation of new tools for monitoring and manipulating basic cellular processes. For example ,
90 genetically encoded voltage sensor (GEVI) designers immediately took advantage of the VSD from
91 Ci-VSP by connecting a fluorescent protein directly to the Ci-VSD (27–29). These new generation
92 GEVIs have significantly improved their signal-to-noise ratio allowing researchers to optically
93 monitor single action potentials (30, 31). Interestingly, the dimerization of fluorescent proteins is
94 known to impact how GEVIs respond to voltage and Ci-VSD dimerization has been used to design
95 intermolecular Förster resonance energy transfer (FRET) GEVIs (32). The Ci-VSD has also been
96 attached to other proteins like the “phosphatase and tensin homolog deleted on chromosome 10”
97 (PTEN) (33). While VSP is a PTEN homologue, PTEN is not voltage dependent so the ability to
98 confer voltage dependence onto PTEN indicates the ability to transfer voltage regulation to create
99 new tools for manipulating intracellular reactions. Along the same lines, groups are engineering
100 other VSPs like Dr-VSP to generate a tool for precisely manipulating PIP concentrations in the cell
101 (11, 34). Understanding how S1 modulates the VSDs will improve the rational design of future VSD-
102 based biosensor tools.
103

104 Our current study set out to investigate the contribution of S1 to VSP function. We found that
105 individual mutations in S1 altered the enzyme activity by altering the amount of catalysis, kinetics,
106 and voltage dependence. The same mutations also changed the kinetics and voltage dependence
107 of the S4 motions as measured by voltage clamp fluorometry. When four S1 mutations were
108 combined, further alterations were observed with the enzymatic activity shifted to higher voltages
109 while the S4 motions were shifted to lower voltages suggesting a decoupling between the VSD and
110 enzyme. When introduced into a GEVI that utilizes the Ci-VSD, the voltage sensitivity and kinetics
111 of the fluorescent signal were also shifted. Thus, S1 plays a strong role in VSP and VSD function.
112

113 **Methods**

114 **Molecular Biology**

115 The Ci-VSP in pSD64TF vector was kindly provided by Y. Okamura (Osaka University, Osaka,
116 Japan). fPLC and fTAPP were both kindly provided by E.Y. Isacoff (University of California,
117 Berkeley). The GEVI CC1 was developed by the Baker laboratory (Korea Institute of Science and
118 Technology) (31). All mutations and N-terminal epitope tags were added using Pfu Turbo
119 polymerase (Agilent). Primers are listed in Supplemental Table 1. All DNA was confirmed by
120 sequencing from start to stop codon. cRNA was transcribed using SP6 or T7 mMessage mMachine
121 (Ambion) kits.
122

123 **Defolliculating *Xenopus laevis* oocytes**

124 *X. laevis* ovaries were purchased from Xenopus One (Dexter, MI). Briefly, each ovary was washed
125 and then morselized in Ca^{2+}-free buffer (96 mM NaCl, 2 mM KCl, 1 mM $MgCl_2$, and 10 mM HEPES,
126 pH 7.6). The morselized ovary was washed in Ca^{2+}-free buffer to remove yolk from lysed oocytes
127 and then digested at room temperature with gentle shaking for 60-70 minutes in 0.5 mg/ml
128 collagenase type 2 (Worthington Biochemical Corporation, catalog # LS004177), and 0.83 mg/ml
129 collagenase type 3 (Worthington Biochemical Corporation, catalog # LS004183) made in Ca^{2+}-free

130 buffer. Post-digestion, the oocytes were washed in Ca^{2+}-free buffer at least 10 times to remove
131 follicles. The oocytes were then sorted and cultured in ND-96 (96 mM NaCl, 2 mM KCl, 1.8 mM
132 $CaCl_2$, 1 mM $MgCl_2$, 50 µg/ml gentamicin, 2.5 mM sodium pyruvate, and 10 mM HEPES, pH 7.6) at
133 18°C.
134
135 **Voltage Clamp Fluorometry**
136 Voltage clamp fluorometry (VCF) was performed as described previously (9). Briefly, *X. laevis*
137 oocytes were injected with 50 nl of 0.4-0.8 µg/µl of cRNA and incubated in ND-96 at 18°C for 24-36
138 hrs. The cRNA dilutions were checked by Nanodrop to ensure the concentrations of total cRNA
139 were correct. On the day of the experiment, oocytes were labeled with tetramethylrhodamine-6-
140 maleimide (TMRM, Invitrogen or Abcam) at a final concentration of 25 µM and the cells were left in
141 the dark on ice for 20 minutes. Labeled oocytes were then extensively washed and stored in ND-
142 96(-) (ND-96 without gentamicin or pyruvate) at 18-19°C until the end of the experiment. A Leica
143 DM IRBE inverted microscope with a Leica HC PI APO 20×/0.7 fluorescence objective was used
144 with a Dagan CA-1B amplifier (Dagan Corporation) and illuminated with a Lumen Dynamics X-Cite
145 XLED1 light source. Fluorescence was measured with a ThorLabs photomultiplier tube (PMT). The
146 amplifier and LED were controlled by a Digidata-1440A board and pClamp10.3 software package
147 (Axon Instruments). Light was filtered through an HQ531/40 excitation filter, an HQ593/40 emission
148 filter and a Q562LP dichroic (Semrock). Fluorescence signals were low-pass filtered at 500 Hz
149 through an eight-pole Bessel filter (Frequency Devices). Glass capillary tubes (VWR) were pulled
150 by a gravity puller (Hamamatsu) for pipette resistances of 0.2-1 MΩ. The VCF voltage protocol
151 consisted of 10 mV steps starting at -150 mV and ending at 200 mV with a holding potential of -80
152 mV. The measured fluorescence was then plotted against the applied voltage to generate the
153 fluorescence/voltage relationship. All microscopes and optics for electrophysiology and
154 fluorescence measurements were placed on a vibration isolation platform (Newport and TMC) to
155 avoid any vibrational noise and homemade Faraday cages were used to avoid electrical noise.

156

157 **Two electrode voltage clamp electrophysiology & optical measurement of enzymatic activity**

158 Two electrode voltage clamp (TEVC) was performed as previously described (9). FRET-based PIP
159 sensors (35, 36) were used to measure depletion of PI(4,5)P_2 or the production and depletion of
160 PI(3,4)P_2. Specifically, we used the PH domain from phospholipase C (PLC) for PI(4,5)P_2 and the
161 PH domain from the tandem PH domain containing protein 1 (TAPP) for PI(3,4)P_2. The FRET
162 sensors were designed with an N-terminal CFP and a C-terminal YFP and were called fPLC and
163 fTAPP respectively. To measure production of PI(4,5)P_2, the diffusion-based sensor GFP-PLC-PH
164 domain (gPLC) was used which has a GFP attached to the N-terminus of the PLC-PH domain. *X.*
165 *laevis* oocytes were injected with cRNA mixtures of VSP and biosensor (0.4/0.4 µg/µl for VSP/fPLC;
166 0.2/0.1 µg/µl for VSP/gPLC; and 0.2/0.4 µg/µl for VSP/fTAPP). The cRNA mixtures were checked
167 by Nanodrop to ensure the concentrations of total cRNA were correct. All VSP constructs for the
168 enzyme activity assays have a TMRM labeling site (G214C) and were tested with VCF to confirm
169 expression. They also have a His-tag to compare with co-immunoprecipitation data. The
170 catalytically inactive Ci-VSP C363S (CS) mutation abolishes catalytic activity and serves as a
171 control for the endogenous *X. laevis* VSP present in oocytes. Each cell was injected with 50 nl
172 cRNA mixtures and then incubated in ND-96 for 24-48 hours at 18-21°C .

173

174 On the day of the experiments, cells were labeled with TMRM as listed under VCF. Post-labeling,
175 oocytes were stored in ND-96(-) containing 8 µM insulin to promote PI3 kinase activity and up
176 regulate PI(3,4,5)P_3 levels. To control for variations in Ci-VSP expression, we tested each cell for
177 VSD motions via VCF as described above. If no VCF was observed, the cell did not move forward
178 for activity testing. For the FRET experiments, light was filtered through a HQ436/20 excitation filter
179 and directed to the objective with a 455LP dichroic (Chroma). The microscope cube did not contain
180 an emission filter, because the ThorLabs PMT module contains its own cube with a 510-nm
181 dichroic, an HQ480/40 emission filter for CFP, and an HQ535/30 emission filter for YFP (Chroma).

182 For the gPLC experiments, light was filtered through a HQ470/40 excitation filter, an HQ525/50
183 emission filter and a Q496LP dichroic (Chroma). The voltage protocol consisted of steps from -100
184 mV to +180 mV in irregular increments. Rest periods of 1-5 minutes between voltage steps were
185 used to allow the cell to recover depleted PIP concentrations before the next voltage step. The
186 length of the voltage pulse was varied for each biosensor, 2-10 s for fTAPP, 2-20 s for fPLC, and
187 1.5-3 s for gPLC. The resulting fluorescence was then plotted vs. voltage to generate the FV
188 relationship.
189
190 **Sensing Currents**
191 Defolliculated *Xenopus laevis* oocytes were injected with 50 nl of 0.8 µg/µl (checked by Nanodrop)
192 cRNA of each Ci-VSP S1 mutation, with the TMRM labeling site mutation (G214C) and a His-tag.
193 These cells were then incubated in ND-96 at 18°C for 24-36 hrs. Oocytes were labeled with 25 µM
194 TMRM as described in the VCF methods. After labeling, oocytes were held & tested in ND-96(-) + 8
195 µM insulin as in the enzymatic activity measurements. The VCF setup used was as described in the
196 VCF methods and all recordings were done at room temperature (22-24°C). The sensing currents
197 were elicited by a 300 ms depolarizing pulse to +150 mV from a holding of -80 mV. The off-sensing
198 current was integrated from the end of the pulse for 150 ms after the pulse. This maximum charge
199 was plotted for each mutation and WT. Leak subtraction was performed by a P/-8 protocol. The
200 simultaneously collected fluorescence was calculated as $\Delta F/F = ((Fx-F0)/F0)$. The absolute value
201 of both the charge and fluorescence data was plotted. Each construct was tested in at least 10
202 oocytes from at least 3 biological variable batches of frogs.
203
204 **Antibodies and Antibody beads**

205 6x-His epitope tag antibody (His.H8) was purchased from Invitrogen. Monoclonal Flag M2 antibody
206 (F1804-50UG), anti-Flag M2 affinity gel (A2220-1ML) were purchased from Sigma-Aldrich. Goat
207 anti-mouse light chain only HRP was purchased from Jackson Labs (115-035-174).
208
209 **Co-immunoprecipitation (co-IP)**
210 Oocytes were injected with 50 nl of 0.4-0.8µg/µL of total cRNA for each construct. Individual
211 constructs were at 0.4 µg/µL and mixtures at 0.4/0.4 µg/µL. The cRNA dilutions and mixtures were
212 checked by Nanodrop to ensure the concentrations of total cRNA were correct. Oocytes were
213 incubated for 24-36 hours in ND-96 at 18-21°C. Protein expression was confirmed using voltage
214 clamp fluorometry. Post-expression check, 1-2 oocytes of those injected with a single RNA and 2-3
215 oocytes of those injected with two RNAs were lysed in 200 µl of lysis buffer (150 mM NaCl, 0.1%
216 IGEPAL, 50 mM Tris-base, pH 7.4 with protease inhibitors). The lysates were centrifuged at
217 21,100g for 15 minutes at 4°C. Supernatant (160 µl) was split into two parts (one aliquot of 130 µl
218 and one aliquot of 30 µl). The anti-FLAG beads in lysis buffer (100 µl, 1:20 ratio) were added to the
219 130 µl sample aliquot. These mixtures were left on a rotator overnight at 4°C. The 30 µl aliquot was
220 stored at -20°C and used as an input control. The samples with the beads were then centrifuged at
221 1,200g for 5 minutes at 4°C to pellet the beads. The supernatant was discarded, and the beads
222 were washed with lysis buffer five times. After the last wash, 7 µl of 3X Laemmli sample buffer was
223 added directly to the beads. To the input control, 7 µl of 5X Laemmli sample buffer was added, and
224 all samples were incubated for 5 minutes at 98°C. The samples were loaded on a 10% SDS-
225 polyacrylamide gel (10 µl/lane) and electrophoresed at 200 mV for about 45 minutes until the
226 bromophenol blue in the sample buffer reached the bottom of the gel.
227
228 **Western blotting**
229 The samples were transferred from the polyacrylamide gel onto a nitrocellulose membrane at 350
230 mA for 70 minutes using a sodium borate buffer system. Post-transfer, the membranes were

231 incubated in blocking buffer (5% milk in 1X TBS-T) for 30 minutes. The membranes were then
232 incubated with the primary antibody solutions (1:2,000 dilution prepared in blocking buffer) 1 hour at
233 room temperature. Membranes were washed 6-8 times with 1X TBS-T over a period of about 1 hr.
234 Secondary antibody solutions prepared in blocking buffer (1:15,000 dilution) were added to the
235 membranes and incubated for 1 hour at room temperature. Washes with 1X-TBS-T were repeated
236 6-8 times. Membranes were developed using WesternBright ECL reagent (Advansta).
237
238 **Patch clamp electrophysiology: Voltage imaging with GEVIs**
239 The original CC1 construct with super ecliptic pHluorin (SE) A227D (31) or CC1 variants with
240 mutations in S1 were expressed in HEK 293 cells via lipofectamine (Invitrogen). Coverslips with
241 transiently transfected cells were placed into a bath chamber (Warner instruments, USA) kept at
242 34° C throughout the experiment and perfused with bath solution (150 mM NaCl, 4 mM KCl, 1 mM
243 $MgCl_2$, 2 mM $CaCl_2$, 5 mM D-glucose and 5 mM HEPES, pH = 7.4). Filamented glass capillary
244 tubes (1.5 mm/0.84 mm; World Precision Instruments, USA) were pulled by a micropipette puller
245 (Sutter, USA) prior to each experiment with pipette resistances of 3–5 MΩ. The pipettes were filled
246 with intracellular solution (120 mM K-aspartate, 4 mM NaCl, 4 mM $MgCl_2$, 1 mM $CaCl_2$, 10 mM
247 EGTA, 3 mM Na_2ATP and 5 mM HEPES, pH = 7.2). Whole cell voltage clamp was conducted using
248 a patch clamp amplifier (HEKA, Germany). A holding potential of −70 mV was used for all
249 recordings.
250
251 An inverted microscope (IX71; Olympus, Japan) equipped with a 60X oil-immersion lens with 1.35-
252 numerical aperture was used for epifluorescence imaging. The light source was a 75 W Xenon arc
253 lamp (Osram, Germany) placed in a lamp housing (Cairn, UK). GFP was imaged using a filter cube
254 consisting of an excitation filter (FF02-472/30-25), a dichroic mirror (FF495-Di03) and an emission
255 filter (FF01-496) for the 470 nm wavelength excitation (Semrock, USA). Fluorescence changes of
256 the voltage indicators were typically recorded at 1 kHz frame rate by a high-speed CCD camera

257 (RedShirtImaging, USA). All the relevant optical devices were placed on a vibration isolation
258 platform (Kinetic Systems, USA) to avoid any vibrational noise during patch clamp fluorometry
259 experiments.
260
261 **Data analysis**
262 ChimeraX was used to visualize the structure of the Ci-VSD (21, 37). Axon™ Clampfit™ 10.3
263 (Molecular Devices) was used to initially process the fluorescence and FRET data. For the VCF, the
264 fluorescence baseline was zeroed and then the amplitude of each pulse measured. The voltages
265 for each pulse were measured. The expression VCF data was calculated as $\Delta F/F = ((Fx-F0)/F0)$.
266 Current data was processed in Clampfit™. Statics were performed in Microsoft Excel with the
267 Student's test calculated as two-tailed and used for equal variance data while the Welsh's t-test was
268 calculated as two-tailed and used for unequal variance data. The FRET ratio was also calculated in
269 Clampfit™. Subsequent analysis of the TEVC activity data was automated using an R script in R
270 Studio. Specifically, for the FRET or fluorescence increase (fTAPP and gPLC, respectively), the
271 activity $\Delta F/F$ was calculated from the pre-pulse baseline to the max signal increase. For the fPLC
272 FRET decrease, the activity $\Delta F/F$ was calculated from the pre-pulse baseline to the max FRET
273 decrease. For the fTAPP FRET decrease, the activity $\Delta F/F$ was calculated from the max FRET
274 increase to the max FRET decrease. In some instances, oocytes injected with catalytically inactive
275 Ci-VSP C363S showed significant background activity indicating that the native *X. laevis* VSP was
276 contributing to the activity signal (36, 38). For those traces, we subtracted an average trace from
277 oocytes expressing C363S from the traces for oocytes expressing wildtype (WT) and the mutant Ci-
278 VSP. All final data were plotted in Igor Pro. Final voltage dependent curves were plotted with
279 change in FRET or fluorescence on the Y-axis and measured voltage on the X-axis. Igor Pro was
280 used to calculate all fits: single or double Boltzmann sigmoid, single or double exponentials and
281 residuals. Activity assays were repeated on oocytes extracted on different days from at least three
282 different frogs (biological replicates) until data from a minimum of 8 oocytes were acquired and

283 analyzed. Error bars indicate standard error of the mean (SEM). Figures were made in Illustrator
284 (Adobe).
285
286 For the patch fluorometry experiments, images were acquired by NeuroPlex (RedShirtImaging,
287 USA) and analyzed for initial parameters such as fluorescence change [ΔF = Fx−F0] or fractional
288 fluorescence change values (ΔF/F = ((Fx−F0)/F0) * 100) by Microsoft Excel. The acquired data
289 from whole cell voltage clamp experiments of HEK 293 cells were averaged for 16 trials. Data were
290 collected from recorded cells that did not lose their seals during the whole cell voltage clamp
291 recording. ΔF/F values for the tested voltage pulses were plotted using Igor Pro.
292
293 **Results**
294 To determine the role S1 helix plays in Ci-VSP function, we started with the Ci-VSD crystal
295 structure that was solved in a dimer conformation (21). Specifically, the biological unit of the
296 structure showed two adjacent VSDs with the S1 and S4 helices of one subunit facing the S1 and
297 S4 helices of the other subunit. This conformation is consistent with a subsequent study from our
298 lab that found that full length Ci-VSP is able to dimerize at high concentrations (22). The same
299 study showed that both the VSD and the phosphatase domain can dimerize independently,
300 suggesting the overall organization of the dimer could be a side-by-side orientation with both
301 domains involved in dimerizing the full length VSP (Fig 1C). We chose to manipulate sites on S1
302 that lined the interface between the two subunits, F127, I131, I134 and L137, for two reasons (Fig
303 1D). First, we expect dimers to influence Ci-VSP activity as seen previously (22) so we wanted to
304 test positions that may be involved in transmitting information across the dimer. Second, we wanted
305 to minimize directly altering the S4 contact points between S1 and S4 (either intra or intersubunit).
306 Of the selected sites, both the F127 and I134 positions exhibit a high conservation of hydrophobic
307 residues across different species homologs of VSPs (Fig 1E). L137 is nearly invariable across

308 different VSPs, while I131 is more tolerant of hydrophobic substitutions (I, F, and V) and hydrophilic
309 (T) residues found in the equivalent positions.
310
311 First, we tested the impact of the individual mutations on the enzymatic activity. Pleckstrin
312 homology (PH) domains from the tandem PH domain-containing protein 1 (TAPP) and from
313 phospholipase C (PLC) selectively bind PI(3,4)P_2 and PI(4,5)P_2 respectively, making them ideal
314 sensors for Ci-VSP activity. We used two different biosensor designs with these PH domains, one
315 where the signal is dependent on a Förster resonance energy transfer (FRET) signal and one
316 where the signal is dependent on the free diffusion of the PH domain (diffusion based). The TAPP
317 FRET sensor, called fTAPP, has an N-terminal CFP followed by the TAPP-PH domain and then a
318 C-terminal YFP with a prenylation site for membrane localization (Fig 2A) (35, 39). An increase in
319 FRET follows the 5-phosphatase reaction of PI(3,4,5)P_3 to PI(3,4)P_2 while a decrease in FRET
320 indicates the 3-phosphatase reaction of PI(3,4)P_2 to PI(4)P (Fig 2A). To increase the amount of
321 PI(3,4,5)P_3 in the cells, all enzymatic activity is recorded in a solution of insulin to activate the
322 endogenous insulin receptor and the subsequent phosphatidyl-3-kinase. WT Ci-VSP gives a robust
323 increase and decrease in FRET when tested with fTAPP consistent with previous publications (Fig
324 2B) (11, 22, 35). Because *X. laevis* oocytes are known to express endogenous VSPs (Xl-VSP1 & 2)
325 (7, 9, 36), a negative control is also needed. Previously, we used an inactive Ci-VSP using the
326 catalytic site mutation, C363S (CS), to mimic our experimental conditions (9, 22, 40). Others use
327 the fTAPP sensor alone to measure endogenous Xl-VSP (8, 11). Since a side-by-side comparison
328 had not been done to our knowledge, we tested both CS with fTAPP and fTAPP alone using long,
329 10 seconds pulses. We found that the CS with fTAPP resulted in statistically higher Xl-VSP activity
330 compared to fTAPP alone (Supp Fig 1A) countering the idea that the two conditions are equivalent.
331 Interestingly, our previous research on the Xl-VSPs showed that Xl-VSP1 can catalyze both
332 PI(3,4,5)P_3 and PI(3,4)P_2 as substrates while Xl-VSP2 is only active against PI(3,4,5)P_3 as a
333 substrate. These results suggest that Xl-VSP2 may dominate the endogenous VSP signal since we

334 only see activity against PI(3,4,5)P_3. Because of the observed difference when CS was expressed,
335 we co-expressed the sensors with CS to control for our experimental conditions more accurately.
336 As seen before, we observe only a small amount of signal coming from endogenous Xl-VSPs when
337 we use 2s depolarizations since the kinetics of the Xl-VSP2 are very slow (Fig 2B, C) (22, 36).
338
339 When testing the S1 mutations, the kinetics for the F127A and I134A mutations were very similar to
340 those of WT (Fig 2B). The voltage dependence for F127A was similar for the 5-phosphatase
341 reaction while slightly shifted to lower voltages for the 3-phosphatase activity (Fig 2C, Table 1).
342 I134A showed a higher voltage requirement for the 5-phosphtase reaction and a slightly lower
343 voltage requirement for the 3-phosphtase reaction. Interestingly, I131A, which is the most variable
344 position (Fig 1E), also showed similar kinetics but with a shift to more positive potentials for both
345 reactions, indicating this position's variability could be part of tuning the voltage dependence
346 between species. The highly conserved L137 position meanwhile dramatically changed activity
347 when mutated to an alanine. The 5-phosphatase activity was greatly reduced, and the 3-
348 phosphatase activity was not visible using a 2s voltage step (Fig 2B, C). However, when the pulse
349 was extended out to 5s, a small 3-phosphatase activity was seen, indicating that the L137A did not
350 eliminate the 3-phosphatase activity but significantly slowed down the reaction compared to the 5-
351 phosphatase reaction (Supp Fig 1B). The longer pulses also resulted in significantly higher
352 endogenous VSP activity as measured by the inactive CS mutation (Supp Fig 1B), obscuring the
353 true activity of the L137A. To compensate for the endogenous activity, we subtracted the CS data
354 from the L137A and WT data, as was done previously (40). The resulting traces showed a robust
355 though slower decrease in FRET when compared to WT (Fig 2D), indicating both reactions are still
356 present. Interestingly, both reactions are significantly shifted to higher voltages and are reduced in
357 magnitude compared to WT (Fig 2E). The 5-phosphatase reaction appears to approach a more
358 linear relationship with voltage, with its larger slope suggesting a weaker sensitivity to voltage and
359 potentially weaker coupling between the VSD and the enzyme or between dimers. The 3-

360 phosphatase reaction retains a clearer sigmoidal relationship with voltage. The strong impact of
361 mutating L137 is consistent with it being well conserved across species and indicates that leucine in
362 position 137 plays a significant role in modulating VSP function (Fig 1E).
363
364 When all four mutations were combined in S1-Q and tested at 2s pulses, the 3-phosphatase activity
365 was not visible, similar to the L137A data (Supp Fig 1C). The 5-phosphatase activity was greatly
366 reduced though still above the CS negative control (Supp Fig 1D). Longer 10s pulses revealed 3-
367 phosphatase activity (Supp Fig 1E), with the endogenous Xl-VSPs giving a large signal that
368 obscures the impact of S1-Q. As with the L137A alone data, we subtracted the CS background from
369 the WT and S1-Q longer pulses. The resulting traces show both reactions clearly though with much
370 slower kinetics (Fig 2F). Interestingly, while the 5s pulses did not dramatically change the WT
371 response, the 10s pulses shifted the WT voltage dependence to higher voltages for the 5-
372 phosphatase reaction and the 3-phosphatase reaction remained similar (Fig 2G, Table 1). For the
373 S1-Q mutation, its 5-phosphatase reaction gives a similar voltage dependence to WT though the
374 amplitude is significantly reduced. The S1-Q 3-phosphatase reaction is shifted to higher potentials
375 as well (Table 1). These data show the importance of helices other than S4 to modulate the ability
376 of the phosphatase to catalyze reactions. It also demonstrates the importance of different pulse
377 lengths for characterizing VSP function.
378
379 The design of the PLC FRET based biosensor, fPLC, is similar to that of fTAPP but the PH domain
380 from PLC is used instead since PLC-PH is selective for $PI(4,5)P_2$ (Fig 3A). We did not use fPLC to
381 quantify the production of $PI(4,5)P_2$ from $PI(3,4,5)P_3$ because, in our hands (and others) the signal
382 is too low for reliable quantification in individual traces (11, 22, 36). However, fPLC is still a good
383 and fast biosensor for quantitating the 5-phosphatase reaction, from $PI(4,5)P_2$ to PI(4)P, via a
384 decrease in the FRET signal (Fig 3A). Thus, using fPLC, we observed the expected FRET
385 decrease with WT and little to no FRET decrease with the CS negative control (Fig 3B). We found

386 that both I131A and I134A had similar fPLC activity kinetics compared to WT while F127A and
387 L137A were slower. L137A also had lower overall activity and was significantly shifted to more
388 positive voltages (Fig 3B, C, Table 2). F127A and I134A had similar voltage dependent activities
389 compared to WT while I131A was again shifted to higher voltages. When S1-Q was tested with
390 fPLC using a 2s pulse, it appeared that the mutation eliminated all activity (Supp Fig 1F). When a
391 significantly longer pulse was given (20s), we did observe a small amount of PI(4,5)P_2 to PI(4)P
392 activity above the negative control values though it was slower, reduced and right shifted (Fig 3D,
393 E, Table 2). Overall, the fPLC data is similar to the fTAPP data in that the most dramatics impacts
394 are from the L137A alone mutation and the S1-Q combination. Both slow down the kinetics with S1-
395 Q significantly slower than L137A even and both shift the voltage dependence to much higher
396 potentials.
397
398 To monitor the production of PI(4,5)P_2 from PI(3,4,5)P_3, we used the diffusion based GFP-PLC-PH
399 biosensor (gPLC), where the increase in fluorescence at the membrane indicates production of
400 PI(4,5)P_2 from PI(3,4,5)P_3 (Fig 4A) (9, 41). As seen previously, WT gives a robust gPLC
401 fluorescence increase and CS shows no endogenous Xl-VSP signal using either a 1.5s or a 3s
402 depolarization (Fig 4B). However, we see a different overall pattern for the mutations compared to
403 the previous biosensors. With the S1 mutations, we found that F127A, I131A and L137A are slower
404 than WT with L137A requiring a longer 3s pulse to see the full signal (Fig 4B). Interestingly, L137A
405 has not lost as much overall activity or voltage dependence as is seen with the other reactions (Fig
406 4C). Both F127A and I131A shifted the voltage dependence of activity to higher voltages, requiring
407 more energy to activate while L137A slightly shifted the voltage dependence to lower voltages (Fig
408 4C, Table 2). I134A has similar kinetics and voltage activation compared to WT, however it appears
409 more active than WT with a larger amplitude fluorescence change. When all four mutations were
410 combined in S1-Q, we observed dephosphorylation at the 3-phosphate from PI(3,4,5)P_3 again with
411 slower kinetics (Fig 4D). The voltage dependence of S1-Q appears significantly shifted to higher

412 voltages and shows a significantly smaller amount of catalysis (Fig 4E). These results indicate that
413 the identity of the substrate is important for voltage dependent catalysis. In addition, the $PI(3,4,5)P_3$
414 to $PI(4,5)P_2$ reaction was quite different for the individual S1 mutation compared to the other
415 biosensors while the S1-Q catalysis was more like the other S1-Q reactions.
416
417 Before each activity assay, every cell was tested for a VCF signal to ensure that the VSP was
418 expressed on the membrane. If no VCF signal was observed, the cell was discarded and another
419 one was tested. All this expression data was compiled and no significant difference was observed
420 for the VCF signal from each mutation when compared to WT (Supp Fig 2A). VCF is well
421 established to monitor both the sensing current and subsequent protein confirmational changes
422 leading to the relaxed state of the VSD (4). VCF does have limitations, however. Very small
423 amounts of protein will not give a fluorescence signal and Western blots are needed to establish
424 protein expression (22). In addition, the amount of protein on the membrane is not easily
425 quantitated from the fluorescence change. When Ci-VSP is expressed at very low concentrations,
426 the activities are known to become shifted to lower voltages (22). To ensure our changes in voltage
427 dependent activity were due to intrinsic properties of the mutation and not as a result of significantly
428 lower protein expression, we also tested the sensing charge movement and VCF signal from the
429 same cells for each mutant (Supp Fig 2B,C). We found that three mutations showed less sensing
430 charge than WT, F127A, I134A and S1-Q, suggesting that these proteins were not as abundant on
431 the membrane compared to WT. However, the VCF signals from all the same cells were similar to
432 WT except for CS and S1-Q which gave larger fluorescence values than WT. Thus, the lower
433 expression does not account for the observed shifts in activity.
434
435 Using voltage clamp fluorometry (VCF), we then tested how each individual mutation impacted VSD
436 motions. We used the common labeling site, G214C, in the S3-S4 loop since it has been shown to
437 be a good reporter of both sensing charge movement and VSD motions (3, 4). The activation

438 kinetics for WT and all the mutations were well fit by a double exponential as previously reported
439 (Fig 5A, Supp Table 2) (3, 4). We found that the first rate, τ_{a1} which is correlated with the sensing
440 charges, are similar between WT and all the single mutations (Supp Table 2). However, the second
441 rate, τ_{a2} which is correlated with the VSD relaxed state, was slightly faster in both F127A and L137A
442 compared to WT (Supp Table 2). We further analyzed the F127A and L137A kinetics across all the
443 tested voltages and found a slightly faster τ_{a1} across multiple voltages (Supp Fig 3A). However, the
444 overall voltage dependence of either rate (τ_{a1} or τ_{a2}) was not significantly different. The
445 repolarization kinetics for F127A, I131A and I134A were similar to WT and were well described by
446 single exponential fits, suggesting that overall, they don't significantly influence the kinetics of S4
447 motions. However, the repolarization kinetics for L137A were slower and better fit by a double
448 exponential, where the first rate, τ_{r1}, is similar to WT and the second rate, τ_{r2}, was significantly
449 slower (Fig 5A, Supp Table 2, Supp Fig 3B). Interestingly, τ_{r1} consistently slowed from 0 to 70 mV
450 for both WT and L137A. Above 70 mV, τ_{r1} stayed the same indicating no further voltage
451 dependence. The second repolarization rate, τ_{r2}, for L137A was also not dependent on voltage and
452 could represent an added step for the VSD to exit the relaxed state. In addition to the kinetic
453 differences, each individual S1 mutation lowered the voltage dependence of the steady state
454 motions, and they were all best fit by a double Boltzmann sigmoid (Fig 5B, Table 3). To confirm the
455 double Boltzmann sigmoid was required, we calculated the residuals for each trace and found that
456 the double sigmoid consistently fit the data better than the single sigmoid (Supp Fig 3C). These
457 results suggest that S1 directly impacts the kinetic and voltage dependent motions of S4. Both
458 F127A and L137A shifted the voltage dependence of $V1_{1/2}$ to lower voltages, by 81 and 72 mV
459 respectively. Interestingly, F127A $V2_{1/2}$ corresponds well with the WT single $V_{1/2}$ while L137A $V2_{1/2}$
460 shifted to higher voltages by 28 mV. Both I131A and I134A shifted $V1_{1/2}$ to lower voltages by
461 smaller amounts while their $V2_{1/2}$ are also shifted to higher voltages (Table 3).

462

463 When all four mutations were combined in S1-Q, both activation rates, τ_{a1} and τ_{a2}, were slightly
464 faster than WT at 200 mV (Supp Table 2) though that trend was not consistent across multiple
465 voltages (Supp Fig 3A). For repolarization, the S1-Q τ_{r1} appeared slower than WT though the
466 difference was not significant for all voltages (Fig 5C, Supp Fig 3B). Interestingly, the S1-Q τ_{r1}
467 appeared less dependent on voltage particularly in the lower voltages (0-70mV) (Supp Fig 3B). The
468 S1-Q τ_{r2} was not voltage dependent and overall is similar to the L137A τ_{r1}. The S1-Q voltage
469 dependence was also a strongly shifted, double Boltzmann sigmoid with $V1_{1/2}$ shifted by 88 mV to
470 lower voltages and $V2_{1/2}$ shifted by 37 mV to higher voltages (Fig 5D, Table 3).

471

472 Since the amino acids tested were at the interface of the VSD dimer, we needed to know whether
473 the mutations altered dimerization to be able to interpret their impact on VSP. Using His and FLAG
474 tags to differentiate between the two subunits of the dimers (Fig 6A), we pulled down with anti-
475 FLAG beads. They all showed pulldown (Fig 6B), indicating that none of the individual mutations
476 altered Ci-VSP dimerization. We only tested the pulldown of the His subunit with the anti-FLAG
477 beads because we discovered that Ci-VSP occasionally binds nonspecifically to cobalt and nickel
478 beads. S1-Q also showed pull down (n=4). We did observe one blot that did not show any pulldown
479 (n=1) even though the input protein concentrations were similar (Fig 6C). This variability could
480 suggest that the mutations may slightly weaken the interactions between the Ci-VSP subunits, but
481 they do not eliminate them. Thus, these mutations can serve to explore the contribution of S1 to Ci-
482 VSP dimer function without breaking the dimer.

483

484 Given the variable effects of the S1 mutations on catalysis, we examined the effect of the S1
485 mutations in the absence of the phosphatase domain. CC1 is a GEVI that has replaced the
486 phosphatase domain with a modified fluorescent protein (FP) to yield a voltage dependent optical

487 signal (Fig 7A) (31). This sensor changes fluorescence in a voltage dependent manner giving a
488 readout of the VSD activation from the cytosolic side. Interestingly, the activation kinetics observed
489 for each mutation in CC1 are significantly different from WT CC1 (Fig 7B), unlike the VCF data (Fig
490 5A). While CC1 I131A is slow like CC1 WT, CC1 F127A, I134A and L137A activate faster than CC1
491 WT and reach a steady state during the 200 ms pulse (Fig 7B). So, while the motions measured
492 from the top of the S4 helix are similar (Fig 5), the propagated motions through S4 and the linker
493 are different. Similarly, the repolarization kinetics are faster than CC1 WT for CC1 F127A, I134A
494 and L137A while they are slower than CC1 WT for CC1 I131A. Comparing the steady state
495 fluorescence versus voltage relationships for these mutations in CC1, we see that both the CC1
496 L137A and CC1 I131A data appear to be shifted to more negative potentials while the other two
497 mutations, CC1 F127A and CC1 I134A, appear shifted to higher voltages (Fig 7C). Since none of
498 the GEVI variants plateaued in response to stronger depolarization steps, the absolute voltage
499 shifts cannot be quantified. However, the relative shifts suggest that both CC1 I131A and CC1
500 L137A lower the energy needed to move S4, consistent with the VCF data, while CC1 F127A and
501 CC1 I134A require more energy to induce the same change in fluorescence. When we tested CC1
502 S1-Q, we observed faster kinetics compared to CC1 WT and the voltage dependence was shifted
503 to lower voltages. These CC1 results indicate that S1 plays a fundamental role in the function of
504 VSDs independent of the phosphatase domain.
505
506 **Discussion**
507 We investigated how the S1 helix in VSP impacts Ci-VSP function, from its enzymatic activity to the
508 movements of the VSD, by mutating different amino acids along the S1 helix to alanine. We chose
509 positions that are consistently hydrophobic across several species of VSP (F127, I134 and L137) as
510 well as a position that is not as well conserved (I131). We found that these residues influenced the
511 kinetics and voltage dependence of enzymatic activity even though they do not reside within the
512 phosphatase domain. The same positions also tuned the kinetics and voltage dependence of VSD

513 motions measured in two different ways, VCF and GEVIs. These findings clearly show that the VSP
514 S1 helix is an important consideration for both VSD and enzyme function with multiple possible
515 mechanistic explanations (Fig 8).
516
517 An important point to note is that because VSP is not a channel, we use indirect biosensors to
518 observe enzymatic activity. Whether the biosensor is a fluorescently dependent sensor as with the
519 PH domains or the biosensor is a PIP dependent channel, all the measurements are an indirect
520 observation of PIP concentrations. Each type of biosensor has its advantages and disadvantages.
521 Specifically, GFP-PH domains have the disadvantage that they are slow while having the
522 advantage of being able to test all the known reactions catalyzed by VSP. The FRET based PH
523 domain sensors are faster since the post-translational modification places the sensors on the
524 membrane. However, as noted by us and others, fPLC does not give a reliable signal for the
525 PI(3,4,5)P_3 reaction to PI(4,5)P_2 (11, 22, 36). Thus, we used the slower gPLC sensor to monitor that
526 reaction. The question arises why does one biosensor report on the reaction and another does not.
527 We do not expect the absolute binding affinities to be different between the fPLC and gPLC
528 biosensors given that they both use the same PH domain. At the same time, proximity to the
529 membrane will influence the on and off kinetics of binding and alter the apparent affinities. Taking
530 this difference into account, we hypothesize that fPLC is at or close to saturated binding to PI(4,5)P_2
531 at typical plasma membrane concentrations. Thus, fPLC is starting already bound to PI(4,5)P_2 and
532 lacks the dynamic range to report on the VSP PI(3,4,5)P_3 reaction to PI(4,5)P_2. Similarly, when we
533 and other groups have used channels such as Kir2.1, GIRK and KCNQ2/3, the rise in PI(4,5)P_2 is
534 not observed via a change in the channel current (42–44). This lack of a response from the
535 channels could indicate that the channels are already saturated with PI(4,5)P_2 and don't respond to
536 the higher concentrations caused by VSP activation. Several other factors could contribute to the
537 discrepancy with channels. Foremost on that list is the starting condition of the cells. It is well known
538 that PI(3,4,5)P_3 is at low concentrations in resting cells given its prominent role in regulating cell

539 growth making any reactions with PI(3,4,5)P_3 as a substrate difficult to observe. To make the
540 PI(3,4,5)P_3 reactions more observable, we take advantage of the endogenous insulin receptor. We
541 add insulin to our recording solution causing the receptor to activate PI3 kinase, increasing the
542 PI(3,4,5)P_3 concentrations. This increases the signal for both the PI(3,4,5)P_3 to PI(4,5)P_2 reaction
543 and the PI(3,4,5)P_3 to PI(3,4)P_2 reaction. Other important factors to consider are the characteristics
544 of the biosensors. PH domains have a one-to-one stoichiometry for binding to PIPs so cooperativity
545 will not be a factor. For most channels, they bind more than one PIP and, in several cases, the
546 cooperative nature of those interactions will limit the response of the channel until sufficient
547 PI(4,5)P_2 has accumulated. These differences make a cross comparison between fluorescent
548 biosensors and channels quite difficult. As a result, we focus on comparing the activities of
549 mutations using the same biosensors and comparing them to both positive and negative controls.
550
551 With those caveats in mind, we turn to the enzymatic activity where we found that the S1 impacts
552 the enzyme response to voltage. It is important to note that modeling data suggested that the
553 observed voltage dependence of activity using these biosensors is influenced by endogenous non-
554 voltage dependent kinases and phosphatases (45, 46) which will impact the apparent VSP voltage
555 dependence of activity. However, we are comparing the mutations to our WT protein, so the
556 endogenous proteins are present in all the data and are assumed to contribute the same amount in
557 each. Three of the four individual mutations tested showed conservative changes to enzymatic
558 activity, but all showed some impact depending on the reaction being observed. We separated out
559 these differences based on three parameters: the magnitude, the kinetics, and the voltage
560 dependence of the activity. In terms of magnitude, the only major difference was with I134A. More
561 dephosphorylation of PI(3,4,5)P_3 was observed and less dephosphorylation of PI(4,5)P_2 indicating
562 that the I134A mutation would leave more PI(4,5)P_2 on the membrane compared to WT VSP. Both
563 I131A and I134A showed similar activity magnitudes. For the kinetics, F127A slowed down the
564 PI(3,4,5)P_3 to PI(4,5)P_2 reaction and both F127A and I131 slowed the PI(4,5)P_2 to PI(4)P_2

565 reactions. The other kinetics were similar to WT. There was more variability in the voltage
566 dependence of these reactions. I131A shifted the PI(3,4,5)P_3 to PI(3,4)P_2 and PI(3,4)P_2 to PI(4)P
567 reactions to higher voltages while the other two mutations were similar to WT. For the PI(3,4,5)P_3 to
568 PI(4,5)P_2 and PI(4,5)P_2 to PI(4)P_2 reactions, both F127A and I131A were shifted to higher voltages
569 while I134A was similar to WT. While the S4 helix with its charge carrying arginines is well known to
570 impact VSP enzymatic activity (2, 10, 25, 47, 48), the role of S1 in VSP is less well understood.
571 These subtle alterations in enzymatic activity from the individual mutations in S1 indicate that
572 hydrophobic residues in S1 transmit information, finely tuning the phosphatase domain activity.
573
574 The most dramatic change with the single mutations was with position L137 which is conserved
575 across many different species (Fig 1E). By altering the leucine to an alanine, the magnitude of
576 activity was consistently reduced, and the voltage dependence was shifted to higher voltages with
577 some appearing more linear (Fig 3, 4, 5). The kinetics of activation were also much slower than WT
578 regardless of the biosensor used. These results suggest that the L137 position is a key modulator
579 for VSP and is consistent with its location where L137 is found at the top of each S1 helix and
580 serves as a focal point between the two subunits (Fig 8). When all four mutations are combined in
581 S1-Q, the kinetics of all the reactions were also reduced in magnitude, slower and shifted to higher
582 energy. While the S1-Q results appear to be dominated by the L137A mutation, there are
583 differences particularly with the PI(3,4,5)P_3 to PI(4,5)P_2 reaction. Specifically, the magnitude of the
584 S1-Q activity is more severely reduced, and the voltage dependence is also more shifted and more
585 linear compared to the L137A alone (Fig 4). Thus, the combination of all four mutations in S1 work
586 together to modulate the enzymatic activity of the phosphatase domain. Whether these allosteric
587 impacts are a result of inter-subunit interactions or from intramolecular interactions within a single
588 subunit remains to be determined.
589

590 For the direct measurement of VSD motion via VCF, we found the activation kinetics of the alanine
591 mutations followed the expected double exponential rates and were mostly similar to WT with minor
592 differences depending on the voltage tested (Supp Table 2, Fig 5A, C, Supp Fig 3A) (3, 4). Thus,
593 the alanine mutations did not drastically alter the activation motions of S4. While the activation
594 kinetics are well established to represent the sensing currents (τ_{a1}) and the entry into the VSD
595 relaxed state (τ_{a2}), the repolarization kinetics were always found to go through a single smooth
596 transition from activated to rest (τ_{r1}). F127A, I131A and I134A showed that single transition with
597 similar rates to WT (Supp Table 2). Interestingly, both the L137A alone and the combination S1-Q
598 introduced a second repolarization transition, τ_{r2}, in addition to the τ_{r1} transition. Addressing the τ_{r1}
599 transitions first, the L137A τ_{r1} transitions were not significantly different from WT across multiple
600 voltages (Supp Fig 3B). We did observe a difference between the τ_{r1} transition between WT and
601 S1-Q at lower voltages but the significance of those differences was not consistent (Supp Fig 3B).
602 The τ_{r2} transitions were similar between L137A alone and S1-Q in that they were not voltage
603 dependent and were significantly slower than the τ_{r1} transition. Given these two characteristics, the
604 τ_{r2} transition could represent a separation between the sensing charge movement and the transition
605 from relaxed to rest. A voltage independent return from relaxed to rest would be consistent with
606 previous findings that showed that the transition between the active to the relaxed state was voltage
607 independent (4). Another possible interpretation could be that since the τ_{r1} values are similar
608 between WT and all the single mutations including L137A, the τ_{r2} transition is due to an additional
609 transition to the sensing charge and relaxed-to-rest transitions, not a separation of the two. Such an
610 additional transition could be due to intersubunit conformational changes between the dimers. Thus,
611 the reason behind the two kinetic repolarization components remains unclear. Further experiments
612 would be needed to explore the additional transition. Next, we plotted the changes in fluorescence
613 against the voltage and found the movement of the mutated positions was separated into two

614 energy transitions, one at low voltage ($V1_{1/2}$) and one at high voltage ($V2_{1/2}$). All the mutations were
615 shifted to lower $V1_{1/2}$ values indicating less energy was needed for the initial movement of S4 (Fig
616 5B, D, Table 3). $V2_{1/2}$ was either similar to WT (F127A) or higher than WT (I131A, I134A, L137A,
617 S1-Q) indicating more energy was needed for the second movement of S4. The $V1_{1/2}$ could
618 correspond to one enzymatic reaction and the $V2_{1/2}$ could correspond to another reaction, but the
619 enzymatic activity doesn't support this interpretation. Instead, this separation into low and high
620 energy movements could come from the dimer interactions where each S1 can modulate the S4
621 from the same subunit and the S4 from the opposing subunit (Fig 8). If this is the case, the results
622 could indicate that one subunit becomes easier to move and the other subunit becomes harder to
623 move as a result of the S1 mutations. Another possible explanation would be that the alanines
624 impacted the hydrophobic "plug" formed between the S1-S3 helices, separating the energetics of
625 S4 into two motions (23). A third explanation could be the loss of an anchor point. Specifically,
626 alanine mutations could allow S1 to move more freely and no longer serve as a counterpoint to the
627 other helices. Further experiments are needed to separate these possible explanations for the two
628 VSD motions and the lower energy requirements. The movement of S4 was clearly altered based
629 on mutations in S1 indicating the influence S1 has over voltage sensing in VSP.
630
631 Interestingly, the GEVI measurement of VSD motion results were quite different than the VCF
632 results. Both CC1 F127A and CC1 I134A required higher voltage, more energy, to move the VSD
633 while CC1 I131A, L137A and S1-Q required less voltage for movement (Fig 7C, E). The observed
634 kinetics are also dramatically different. CC1 I131A was similar to CC1 WT while all the other
635 mutations were significantly faster for activation and repolarization (Fig 7B, D). This variation from
636 the VCF data could stem from the location of the fluorescence reporter. For VCF, the TMRM is
637 located extracellularly between S3 and S4, reporting the extracellular motions of S4, while for the
638 GEVI, the FP is located intracellularly and so will report on the intracellular motions of S4 through
639 the linker to the FP. The variation could also stem from the fluorophores themselves. TMRM is a

640 small chemical which is very sensitive to its local microenvironment so as the S4 helix moves,
641 TMRM will move as well, a direct measure of motion. The FP is an indirect measurement given the
642 voltage change causes a conformational change in S4 which is propagated through the linker to the
643 FP beta barrel altering the chromophore and then altering fluorescence. Lastly, the variation could
644 stem from the VSP dimers. While the impact of dimerization is currently unknown for TMRM,
645 previous reports indicate that the dimerization of GEVIs impacts the output fluorescence (32, 49).
646 Our results clearly show that the design of GEVIs using VSP VSDs should consider S1 modulation
647 when tuning the GEVI for particular properties.
648
649 Previous work analyzed the relaxed state as a mechanism to explain the fluorescence changes in
650 the GEVI VSFP2.3 (29). Specifically, VSFP2.3 consists of a tandem pair of FPs fused to the
651 carboxyl end causing a change in intramolecular FRET when the VSD changes its conformation in
652 response to voltage. The mechanism for CC1 and other ArcLight-derived GEVIs are known to be
653 different. Specifically, there is an intermolecular interaction between the FP domains of neighboring
654 GEVIs. This intermolecular interaction enables the negative charge of the A227D mutation in Super
655 Ecliptic pHluorin to influence the fluorescence of a neighboring chromophore. This interaction of FP
656 domains has been shown by replacing SE with a FRET donor FP and co-transfecting it with a
657 separate GEVI containing a FRET acceptor (49). With both domains (the VSD and the FP)
658 experiencing conformational changes, it is difficult to optically resolve the potential relaxation of the
659 VSD from a conformational change relating to the FP domain.
660
661 Bringing together the enzymatic and VCF data, we see a complicated picture emerge regarding
662 VSD control of the phosphatase. In particular, we note that the double sigmoid needed to fit the
663 VCF data for all the mutations is not observed in the enzymatic activity data. The lower voltage
664 movements ($V1_{1/2}$) are much lower than the activity voltage dependence indicating a discrepancy
665 between activation of the VSD and activation of the enzyme. Additionally, the majority of the mutant

666 enzymatic reactions were shifted to higher voltages, indicating more energy was needed to activate
667 the phosphatase with S1 mutated. These opposite impacts could indicate that the ability of the VSD
668 to control the phosphatase was weaker, making it harder for the VSD to conformationally change
669 the phosphatase into its active form, thus requiring higher voltage for catalysis. Decoupling between
670 the VSD and phosphatase has been seen before using mutations in the linker (7, 42, 50, 51) and in
671 S4 (10) but never before from mutations in the S1 helix. The linker decoupling has been long
672 assumed to be an intramolecular process where the VSD no longer communicates with its
673 phosphatase domain. Given the proposed side by side organization of the VSP dimer (Fig 1C), this
674 interpretation of the data may be over simplified. In addition, the location of both S1 and S4 at the
675 interface of the VSD dimer (21) suggests that the observed decoupling with S1 or S4 mutations
676 could be due to either intramolecular interactions as assumed for the linker decoupling or due to
677 intermolecular interactions. Thus, multiple mechanisms are possible for VSP coupling. For example,
678 following a purely intramolecular mechanism, S1 from subunit “A” directly interacts with S4 from
679 subunit “A” with the same happening within subunit “B” (Fig 8, purple arrows). In this scenario, the
680 phosphatase domain from subunit A would couple only to the VSD from subunit A. Another possible
681 mechanism could be that the S1 from subunit A could influence the S4 from subunit B (Fig 8, black
682 arrows). In this case, phosphatase B would receive a signal from VSD B, but the signal would be
683 influenced by VSD A. Similarly, another mechanism could be direct interactions between the S1s
684 mediating the dimer interface (Fig 8, cyan arrows). This would also lead to a scenario where
685 phosphatase B responds to VSD B but is influenced by VSD A. It is important to note that we are
686 focusing here on the VSD. The phosphatase domains are also known to dimerize (22), so direct
687 interactions between the phosphatases may occur in addition to the VSD interactions. Further
688 experiments will be needed to determine whether the VSD control of the phosphatase is purely
689 intramolecular (intrasubunit), purely intermolecular (intersubunit) or a combination of both.
690

691 Overall, our results indicate that the VSP S1 plays an active role in enzymatic function. Specifically,
692 we show that the S1 helix in VSP impacts both the voltage dependence of catalysis as well as the
693 voltage dependent motions of S4. However, the mechanism behind S1's role is still uncertain. The
694 Hv S1 is believed to mediate both the dimer interface (17–19) and the cooperativity between the
695 two subunits (52, 53). The Hv S1 is also involved in channel opening making it a critical aspect of
696 how Hv functions (20). Further experiments are needed to determine whether these aspects of S1
697 function are true in VSP as well. A better understanding of how S1 helices contribute to VSD
698 function is important for understanding the VSD and VSP as a whole.
699
700 **Figure Legends**
701 Figure 1: A) Cartoon representation of a single VSP subunit with the four transmembrane helices of
702 the VSD in purple (S1-S4) and the phosphatase domain in peach. B) Reactions catalyzed by VSP.
703 Four different reactions with three different substrates. C) Cartoon representation of a possible VSP
704 dimer organization based on previous results showing both the VSD and phosphatase domains
705 involved in dimerization. D) 4G80 Protein data bank structure of Ci-VSD, biological unit, rendered
706 using ChimeraX (37). The structure suggests a specific dimer interface. Ribbon representation of
707 S1-S4 with S1s in orange and S4s in green. Position F127, I131, I134 and L137 shown in space-
708 filling cartoon. E) Alignment of the VSP S1 helices from several species. Arrows indicate the
709 positions to be mutated to alanine. Sequences for alignments: l*aevis*VSP2,
710 gi|325976472|gb|ADZ48071.1; *laevis*VSP1, gi|148230800|ref|NP_001090072.1; *tropicalis*VSP,
711 gi|62859843|ref|NP_001015951.1; macaqueVSP, gi|75076430|sp|Q4R6N0.1; chickenVSP,
712 gi|118084924|ref|XP_417079.2; mouseVSP, gi|76827498|gb|AAI07330.1; ratVSP,
713 gi|157820295|ref|NP_001102347.1; humanVSP2, gi|37788781|gb|AAP45144.1; humanVSP1,
714 gi|213972591|ref|NP_954863.2; zebrafishVSP, gi|70887553|ref|NP_001020629.1; cionaVSP,
715 gi|76253898|ref|NP_001028998.1.
716

717 Figure 2: S1 helix modulates kinetics and voltage dependence of PI(3,4,5)P_3 and PI(3,4)P_2
718 dephosphorylation. A) Cartoon depicting the biosensor fTAPP's expected response to VSP 5-
719 phosphate dephosphorylation from PI(3,4,5)P_3 (increase in FRET) and 3-phosphate
720 dephosphorylation from PI(3,4)P_2 (decrease in FRET). B) Averaged fTAPP data for a voltage step
721 from -100 mV holding potential to 160 mV for 2s for the single S1 mutations (F127A, I131A, I134A
722 and L137A). L137A appears to only show 5-phosphatase activity while the others closely resemble
723 WT kinetics of activity. C) Voltage dependent fTAPP activity for the single S1 mutations. The up-
724 FRET component was separated from the down FRET component (see Materials and Methods).
725 While F127A and I134A are very similar to WT, the I131A mutation shifts the voltage dependence
726 of both reactions to higher voltages and the L137A mutation only displays 5-phosphatase activity
727 with the short 2s steps. D) Averaged data for a longer voltage step (5s) from -100 mV to 160 mV for
728 L137A and WT with the CS control subtracted from each (data without subtraction in Supplemental
729 Fig 1B). A clear FRET decrease is visible for L137A at the longer step, indicating that while the
730 mutation does not eliminate 3-phosphatase activity, it slows it down relative to WT. E) L137A
731 voltage dependent fTAPP activity for the 5s voltage step. Both up and down FRET components are
732 visible though the upward component appears more linear. F) Averaged data for a longer voltage
733 step (10s) from -100 mV to 160 mV for S1-Q and WT with the CS control subtracted from each
734 (data without subtraction in Supplemental Fig 1E). A clear FRET decrease is visible for S1-Q at the
735 longer step, indicating that while the mutation does not eliminate 3-phosphatase activity, it slows it
736 down relative to WT. G) S1-Q and WT voltage dependent fTAPP activity for the 10s voltage step.
737 Both up and down FRET components are visible though the upward component appears more
738 linear. All error bars are ± SEM. Data fit with single Boltzmann sigmoid equations.
739
740 Figure 3: S1 helix impacts kinetics of PI(4,5)P_2 5-phosphate dephosphorylation. A) Cartoon
741 depicting the biosensor fPLC's expected response to VSP 5-phosphate dephosphorylation from
742 PI(4,5)P_2 (decrease in FRET). B) Averaged fPLC data for a 2s voltage step from -100 mV to 160

743 mV for the single S1 mutations (F127A, I131A, I134A and L137A). L137A significantly slowed the 5-
744 phosphatase activity while the other mutations more closely resemble WT kinetics. C) Voltage
745 dependent fPLC activity for the single S1 mutations. The I131A mutation shifts the voltage
746 dependence of activity to higher voltages. The L137A mutation displays reduced and right shifted 5-
747 phosphatase activity. D) Averaged data for a long voltage step (20s) from -100 mV to 160 mV for
748 S1-Q and controls. A FRET decrease is visible for S1-Q at the longer step, indicating that while the
749 mutation does not eliminate 5-phosphatase activity, it significantly slows it down. The CS constructs
750 indicates minimal endogenous Xl-VSP2 activity even with such a long pulse. E) Voltage dependent
751 fPLC activity for S1-Q, WT and CS using the longer (20s) pulses. While S1-Q is still active, the
752 activity is almost linear with voltage dependence. All error bars are ± SEM. Data fit with single
753 Boltzmann sigmoid equations.
754
755 Figure 4: S1 helix modulates the kinetics of PI(3,4,5)P_3 3-phosphate dephosphorylation. A) Cartoon
756 depicting the biosensor gPLC's expected response to VSP 3-phosphate dephosphorylation from
757 PI(3,4,5)P_3 to PI(4,5)P_2 (increased membrane fluorescence). B) Averaged gPLC data for a voltage
758 step from -100 mV to 160 mV for the single S1 mutations (F127A, I131A, I134A and L137A). L137A
759 significantly slowed the 3-phosphatase activity requiring a 3s pulse. C) Voltage dependent gPLC
760 activity for the single S1 mutations. While I134A is similar to WT voltage dependence, it shows an
761 enhanced overall activity. Both the F127A and I131A mutations shift the voltage dependence of
762 activity to higher voltages while L137A displays reduced 3-phosphatase activity and is slightly left
763 shifted though the slope is significantly reduced. D) Averaged data for a voltage step from -100 mV
764 to 160 mV for WT and S1-Q. Slower activation was observed for S1-Q so a 3s pulse was used. E)
765 Voltage dependent gPLC activity for WT and S1-Q. The S1-Q significantly reduced the activity and
766 shifted the voltage dependence to higher voltages, more than just the sum of the individual
767 mutations. All error bars are ± SEM. Data fit with single Boltzmann sigmoid equations.
768

769 Figure 5: S1 helix tunes voltage dependence of S4 motion. A) Representative VCF traces for a
770 voltage step from -80 mV to 200 mV for all individual S1 mutations. Activation and repolarization
771 kinetics are similar to WT except for L137A which has a second, slower repolarization motion. B)
772 Voltage dependence of the VSD motions. Mutations in S1 of VSP shift the voltage dependence of
773 VSD motions to lower voltages and introduce a second component in the motion. WT fit by single
774 Boltzmann sigmoid while mutants are fit by double Boltzmann sigmoid. C) Representative VCF
775 trace for a voltage step from -80 mV to 200 mV for S1-Q and WT. Repolarization kinetics show an
776 additional slower component for S1-Q. D) The voltage dependent motions of S1-Q significantly
777 shifted the voltage dependence of activation by almost 90 mV compared to WT. It also introduced a
778 second component. WT fit by single Boltzmann sigmoid, and S1-Q fit by double Boltzmann sigmoid.
779 All constructs have an N-terminal His-tag to compare with co-IP data. All errors are ± SEM.
780
781 Figure 6. Co-immunoprecipitation pull downs show S1 mutations do not disrupt VSP dimers. A)
782 Cartoon representation of VSP dimers with the His and FLAG tags on the N-terminus. B)
783 Immunoprecipitation assay using individual S1 mutations F127A, I131A, I134A, L137A. Inputs were
784 checked for both FLAG and His to ensure expression. Each blot is representative of at least three
785 pull down blots and shows the FLAG tagged subunit is able to pull down the His-tagged subunit. C)
786 Same experiment with all four mutations on a single subunit, called S1-Q for quad mutation on S1.
787 Top blot shows pull down (representative of four separate experiments) while the bottom blot does
788 not (one blot) even though protein levels are similar between the two.
789
790 Figure 7: A) Cartoon representation of the GEVI CC1 with the VSD from Ci-VSP attached an FP. B)
791 Averaged series of voltage steps showing kinetics of fluorescence change for CC1 WT and S1
792 mutants expressed in HEK293 cells. Faster activation and repolarization kinetics observed for
793 F127A, I134A and L137A. C) Voltage dependent fluorescence change for WT and S1 mutations.
794 F127A and I134A shift the voltage dependence to higher voltages while I131A and L137A shift to

795 lower voltages. D) Averaged data for a series of voltage steps for WT and S1-Q. S1-Q shows
796 consistently faster kinetics. E) Voltage dependent fluorescence change for WT and S1-Q. Strong
797 leftward shift consistent with leftward shift from VCF data. All error bars are ± SEM. Data fit with
798 single Boltzmann sigmoid equations.
799
800 Figure 8. Model for S1 modulation of S4. 4G80 Protein data bank ribbon rendering of Ci-VSD
801 dimers using ChimeraX (37). L137 depicted in red space filling, F127, I131 and I134 depicted in
802 blue space filling, S1 in orange and S4 in green. (left) View is facing into the membrane. S1 from
803 subunit A could be interacting with S4 from subunit B (black arrow) and/or S1 from subunit B (cyan
804 arrow). (middle) Turned in membrane view. Arrows show the same possible interactions. (right)
805 Top-down view shows how the S1 from one subunit can interact with the S4 from the same subunit
806 (purple arrow) as well as the S4 from the adjacent subunit (black arrow). Cyan arrows indicate
807 possible intermolecular interactions through the S1s at the dimer interface between subunits A and
808 B. Black arrows indicate possible intermolecular interactions between the S1 from subunit B to S4
809 from subunit A. Purple arrows indicate possible intramolecular interactions between the S1 and S4
810 of the same subunit.
811
812 **Data are openly available in a public repository.**
813 The data underlying Figure 6 are openly available in Figshare at
814 https://doi.org/10.6084/m9.figshare.23960841.
815
816 **Acknowledgements**
817 We thank Y. Okamura for providing the Ci-VSP cDNA and E.Y. Isacoff for the fPLC and fTAPP.
818 This work was supported by funds from National Institute of General Medical Science of
819 the National Institutes of Health grants R01GM111685 (S.C.K.) and P20GM103474 (G.M., W.B.,
820 M.F., J.J.K. and J.A.D.); National Science Foundation grant 2310489 (S.C.K.); Korea Institute of

821 Science and Technology grant 2E31523 (B.J.B.). Molecular graphics and analyses performed with
822 UCSF ChimeraX, developed by the Resource for Biocomputing, Visualization, and Informatics at
823 the University of California, San Francisco, with support from National Institutes of Health
824 R01GM129325 and the Office of Cyber Infrastructure and Computational Biology, National Institute
825 of Allergy, and Infectious Diseases.
826
827 The authors declare no competing financial interests.
828
829 Author contributions: V.R. and S.C.K. conceived the experiments. V.R., H.M.M., B.B, and S.C.K.
830 designed experiments. V.R., H.M.M., W.B., V.C.Y., M.F., G.M., W.O.R., J.J.K., W.J.R, L.M.L.,
831 J.A.D., B.B, and S.C.K. collected and analyzed data. H.M.M., V.R., V.C.Y., B.B. and S.C.K.
832 interpreted the data. S.C.K. and B.B. drafted and revised the manuscript. All authors approved the
833 final version of the manuscript.
834
835 **References**

836 1. B. Hille, *Ionic Channels of Excitable Membranes*, 3rd Ed. (Sinauer, 2001).

837 2. Y. Murata, H. Iwasaki, M. Sasaki, K. Inaba, Y. Okamura, Phosphoinositide phosphatase activity
838 coupled to an intrinsic voltage sensor. *Nature* **435**, 1239–1243 (2005).

839 3. S. C. Kohout, M. H. Ulbrich, S. C. Bell, E. Y. Isacoff, Subunit organization and functional
840 transitions in Ci-VSP. *Nat. Struct. Mol. Biol.* **15**, 106–108 (2008).

841 4. C. A. Villalba-Galea, W. Sandtner, D. M. Starace, F. Bezanilla, S4-based voltage sensors have
842 three major conformations. *Proc. Natl. Acad. Sci. U. S. A.* **105**, 17600–17607 (2008).

843 5. H. Iwasaki, *et al.*, A voltage-sensing phosphatase, Ci-VSP, which shares sequence identity
844 with PTEN, dephosphorylates phosphatidylinositol 4,5-bisphosphate. *Proc. Natl. Acad. Sci. U.*

845 *S. A.* **105**, 7970–7975 (2008).

846 6. C. R. Halaszovich, D. N. Schreiber, D. Oliver, Ci-VSP is a depolarization-activated
847 phosphatidylinositol-4,5-bisphosphate and phosphatidylinositol-3,4,5-trisphosphate 5'-
848 phosphatase. *J. Biol. Chem.* **284**, 2106–2113 (2009).

849 7. S. C. Kohout, *et al.*, Electrochemical coupling in the voltage-dependent phosphatase Ci-VSP.
850 *Nat. Chem. Biol.* **6**, 369–375 (2010).

851 8. T. Kurokawa, *et al.*, 3' Phosphatase activity toward phosphatidylinositol 3,4-bisphosphate
852 [PI(3,4)P2] by voltage-sensing phosphatase (VSP). *Proceedings of the National Academy of*
853 *Sciences* **109**, 10089–10094 (2012).

854 9. P. M. Castle, K. D. Zolman, S. C. Kohout, Voltage-sensing phosphatase modulation by a C2
855 domain. *Front. Pharmacol.* **6**, 63 (2015).

856 10. N. Mizutani, *et al.*, Interaction between S4 and the phosphatase domain mediates
857 electrochemical coupling in voltage-sensing phosphatase (VSP). *Proc. Natl. Acad. Sci. U. S. A.*
858 **119**, e2200364119 (2022).

859 11. I. C. Paixao, *et al.*, Role of K364 next to the active site cysteine in voltage-dependent
860 phosphatase activity of Ci-VSP. *Biophys. J.* (2023) https:/doi.org/10.1016/j.bpj.2023.01.022.

861 12. J. A. Freites, D. J. Tobias, Voltage Sensing in Membranes: From Macroscopic Currents to
862 Molecular Motions. *J. Membr. Biol.* **248**, 419–430 (2015).

863 13. L. D. Islas, Functional diversity of potassium channel voltage-sensing domains. *Channels*, 00–
864 00 (2016).

865 14. S. A. Seoh, D. Sigg, D. M. Papazian, F. Bezanilla, Voltage-sensing residues in the S2 and S4
866 segments of the Shaker K+ channel. *Neuron* **16**, 1159–1167 (1996).

867 15. D. M. Papazian, *et al.*, Electrostatic interactions of S4 voltage sensor in Shaker K+ channel.
868 *Neuron* **14**, 1293–1301 (1995).

869 16. B. Chanda, F. Bezanilla, A common pathway for charge transport through voltage-sensing
870 domains. *Neuron* **57**, 345–351 (2008).

871 17. L. Hong, V. Singh, H. Wulff, F. Tombola, Interrogation of the intersubunit interface of the open
872 Hv1 proton channel with a probe of allosteric coupling. *Sci. Rep.* **5**, 14077 (2015).

873 18. Q. Li, *et al.*, Resting state of the human proton channel dimer in a lipid bilayer. *Proc. Natl.*
874 *Acad. Sci. U. S. A.*, 201515043 (2015).

875 19. S.-Y. Lee, J. A. Letts, R. Mackinnon, Dimeric subunit stoichiometry of the human voltage-
876 dependent proton channel Hv1. *Proc. Natl. Acad. Sci. U. S. A.* **105**, 7692–7695 (2008).

877 20. L. Mony, T. K. Berger, E. Y. Isacoff, A specialized molecular motion opens the Hv1 voltage-
878 gated proton channel. *Nat. Struct. Mol. Biol.* **22**, 283–290 (2015).

879 21. Q. Li, *et al.*, Structural mechanism of voltage-dependent gating in an isolated voltage-sensing
880 domain. *Nat. Struct. Mol. Biol.* **21**, 244–252 (2014).

881 22. V. Rayaprolu, P. Royal, K. Stengel, G. Sandoz, S. C. Kohout, Dimerization of the voltage-
882 sensing phosphatase controls its voltage-sensing and catalytic activity. *J. Gen. Physiol.* **150**,
883 683–696 (2018).

884 23. J. J. Lacroix, F. Bezanilla, Tuning the voltage-sensor motion with a single residue. *Biophys. J.*
885 **103**, L23–L25 (2012).

886 24. C. R. Halaszovich, *et al.*, A human phospholipid phosphatase activated by a transmembrane
887 control module. *J. Lipid Res.* **53**, 2266–2274 (2012).

888 25. S. Sakata, Y. Okamura, Phosphatase activity of the voltage-sensing phosphatase, VSP, shows
889 graded dependence on the extent of activation of the voltage sensor. *J. Physiol.* **592**, 899–914
890 (2014).

891 26. H. Tsutsui, Y. Jinno, A. Tomita, Y. Okamura, Optically detected structural change in the N-
892 terminal region of the voltage-sensor domain. *Biophys. J.* **105**, 108–115 (2013).

893 27. A. Lundby, H. Mutoh, D. Dimitrov, W. Akemann, T. Knöpfel, Engineering of a genetically
894 encodable fluorescent voltage sensor exploiting fast Ci-VSP voltage-sensing movements.
895 *PLoS One* **3**, e2514 (2008).

896 28. B. J. Baker, *et al.*, Genetically encoded fluorescent sensors of membrane potential. *Brain Cell*
897 *Biol.* **36**, 53–67 (2008).

898 29. C. A. Villalba-Galea, *et al.*, Charge movement of a voltage-sensitive fluorescent protein.
899 *Biophys. J.* **96**, L19-21 (2009).

900 30. L. Barnett, J. Platisa, M. Popovic, V. A. Pieribone, T. Hughes, A fluorescent, genetically-
901 encoded voltage probe capable of resolving action potentials. *PLoS One* **7**, e43454 (2012).

902 31. H. H. Piao, D. Rajakumar, B. E. Kang, E. H. Kim, B. J. Baker, Combinatorial mutagenesis of
903 the voltage-sensing domain enables the optical resolution of action potentials firing at 60 Hz by
904 a genetically encoded fluorescent sensor of membrane potential. *J. Neurosci.* **35**, 372–385
905 (2015).

906 32. B. E. Kang, B. J. Baker, Pado, a fluorescent protein with proton channel activity can optically
907 monitor membrane potential, intracellular pH, and map gap junctions. *Sci. Rep.* **6**, 23865
908 (2016).

909 33. J. Lacroix, *et al.*, Controlling the activity of a phosphatase and tensin homolog (PTEN) by

910 membrane potential. *J. Biol. Chem.* **286**, 17945–17953 (2011).

911 34. A. Kawanabe, *et al.*, Engineering an enhanced voltage-sensing phosphatase. *J. Gen. Physiol.*
912 **152** (2020).

913 35. S. S. Grimm, E. Y. Isacoff, Allosteric substrate switching in a voltage-sensing lipid
914 phosphatase. *Nat. Chem. Biol.* **12**, 261–267 (2016).

915 36. W. Ratzan, V. Rayaprolu, S. E. Killian, R. Bradley, S. C. Kohout, The voltage sensing
916 phosphatase (VSP) localizes to the apical membrane of kidney tubule epithelial cells. *PLoS*
917 *One* **14**, e0209056 (2019).

918 37. E. F. Pettersen, *et al.*, UCSF ChimeraX: Structure visualization for researchers, educators, and
919 developers. *Protein Sci.* **30**, 70–82 (2021).

920 38. W. J. Ratzan, A. V. Evsikov, Y. Okamura, L. A. Jaffe, Voltage sensitive phosphoinositide
921 phosphatases of Xenopus: their tissue distribution and voltage dependence. *J. Cell. Physiol.*
922 **226**, 2740–2746 (2011).

923 39. M. Sato, Y. Ueda, T. Takagi, Y. Umezawa, Production of PtdInsP3 at endomembranes is
924 triggered by receptor endocytosis. *Nat. Cell Biol.* **5**, 1016–1022 (2003).

925 40. L. Liu, *et al.*, A glutamate switch controls voltage-sensitive phosphatase function. *Nat. Struct.*
926 *Mol. Biol.* **19**, 633–641 (2012).

927 41. T. Balla, Phosphoinositides: tiny lipids with giant impact on cell regulation. *Physiol. Rev.* **93**,
928 1019–1137 (2013).

929 42. C. A. Villalba-Galea, F. Miceli, M. Taglialatela, F. Bezanilla, Coupling between the voltage-
930 sensing and phosphatase domains of Ci-VSP. *J. Gen. Physiol.* **134**, 5–14 (2009).

931 43. A. Kawanabe, *et al.*, The hydrophobic nature of a novel membrane interface regulates the
932 enzyme activity of a voltage-sensing phosphatase. *Elife* **7**, 3684 (2018).

933 44. A. Rjasanow, M. G. Leitner, V. Thallmair, C. R. Halaszovich, D. Oliver, Ion channel regulation
934 by phosphoinositides analyzed with VSPs – PI(4,5)P2 affinity, phosphoinositide selectivity, and
935 PI(4,5)P2 pool accessibility. *Front. Pharmacol.* **6**, 127 (2015).

936 45. D. Keum, M. Kruse, D.-I. Kim, B. Hille, B.-C. Suh, Phosphoinositide 5- and 3-phosphatase
937 activities of a voltage-sensing phosphatase in living cells show identical voltage dependence.
938 *Proc. Natl. Acad. Sci. U. S. A.* **113**, E3686-95 (2016).

939 46. M. Kruse, S. C. Kohout, B. Hille, Reinterpretation of the substrate specificity of the voltage-
940 sensing phosphatase during dimerization. *J. Gen. Physiol.* **151**, 258–263 (2019).

941 47. Y. Murata, Y. Okamura, Depolarization activates the phosphoinositide phosphatase Ci-VSP, as
942 detected in Xenopus oocytes coexpressing sensors of PIP2. *J. Physiol.* **583**, 875–889 (2007).

943 48. M. I. Hossain, *et al.*, Enzyme domain affects the movement of the voltage sensor in ascidian
944 and zebrafish voltage-sensing phosphatases. *J. Biol. Chem.* **283**, 18248–18259 (2008).

945 49. L. M. Leong, B. E. Kang, B. J. Baker, Improving the flexibility of genetically encoded voltage
946 indicators via intermolecular FRET. *Biophys. J.* **120**, 1927–1941 (2021).

947 50. K. Hobiger, T. Utesch, M. A. Mroginski, T. Friedrich, Coupling of Ci-VSP modules requires a
948 combination of structure and electrostatics within the linker. *Biophys. J.* **102**, 1313–1322
949 (2012).

950 51. K. Hobiger, T. Utesch, M. A. Mroginski, G. Seebohm, T. Friedrich, The linker pivot in Ci-VSP:
951 the key to unlock catalysis. *PLoS One* **8**, e70272-13 (2013).

952 52. F. Tombola, M. H. Ulbrich, S. C. Kohout, E. Y. Isacoff, The opening of the two pores of the Hv1

953 voltage-gated proton channel is tuned by cooperativity. *Nat. Struct. Mol. Biol.* **17**, 44–50 (2010).

954 53. C. Gonzalez, H. P. Koch, B. M. Drum, H. P. Larsson, Strong cooperativity between subunits in

955 voltage-gated proton channels. *Nat. Struct. Mol. Biol.* **17**, 51–56 (2010).

956 Table 1: fTAPP biosensor activity

			PI(3,4,5)P_3 to PI(3,4)P_2		**PI(3,4)P_2 to PI(4)P**	
	n	**Pulse time (s)**	**$V_{1/2}$ up**	**up slope**	**$V_{1/2}$ down**	**down slope**
WT	21	2	32 ± 2	20 ± 2	94 ± 4	17 ± 3
F127A	8	2	30 ± 2	20 ± 2	72 ± 3	15 ± 2
I131A	9	2	65 ± 3	29 ± 3	124 ± 6	19 ± 4
I134A	8	2	41 ± 2	15 ± 2	82 ± 2	13 ± 2
L137A	8	2	21 ± 10	34 ± 7	ns	ns
S1-Q	8	2	222 ± 554	193 ± 193	ns	ns
WT	9	5	41 ± 4	23 ± 4	92 ± 2	20 ± 2
L137A	13	5	>276	71 ± 45	124 ± 9	36 ± 6
WT	10	10	167 ± 17	62 ± 6	111 ± 4	30 ± 3
S1-Q	9	10	159 ± 40	25 ± 15	140 ± 13	36 ± 6

957 ns= no signal detected

958

959

960

961

962

963

964

965

966

967

968 Table 2: gPLC and fPLC biosensor activity

	gPLC				fPLC			
	$PI(3,4,5)P_3$ to $PI(4,5)P_2$				$PI(4,5)P_2$ to $PI(4)P$			
	n	Pulse time (s)	$V_{1/2}$	slope	n	Pulse time (s)	$V_{1/2}$	slope
WT	20	1.5	90 ± 3	28 ± 2	27	2	92 ± 3	26 ± 3
F127A	8	1.5	137 ± 6	36 ± 3	8	2	104 ± 5	28 ± 4
I131A	9	1.5	104 ± 7	44 ± 5	8	2	125 ± 6	33 ± 4
I134A	9	1.5	89 ± 2	20 ± 1	14	2	81 ± 2	18 ± 2
L137A	8	3	64 ± 7	50 ± 8	9	2	147 ± 14	23 ± 8
S1-Q	9	3	167 ± 20	58 ± 7	11	2	181 ± 91	15 ± 22
WT	N/A	N/A	N/A	N/A	11	20	70.2 ± 0.7	18.0 ± 0.7
S1-Q	N/A	N/A	N/A	N/A	9	20	119 ± 13	44 ± 8

969

970

971 Table 3: VCF, voltage dependent S4 motions

	n	$V1_{1/2}$	slope 1	$V2_{1/2}$	slope 2
WT	10	ns	ns	70.5 ± 0.5	26.5 ± 0.4
F127A	10	-11 ± 4	24 ± 2	76 ± 3	27 ± 1
I131A	13	20 ± 3	25 ± 1	100 ± 5	20 ± 3
I134A	15	37 ± 5	25 ± 1	89 ± 3	16 ± 2
L137A	10	-2 ± 1	21.2 ± 0.7	99 ± 11	23 ± 8
S1-Q	10	-18 ± 2	31 ± 1	108 ± 14	20 ± 12

972 ns= no signal detected

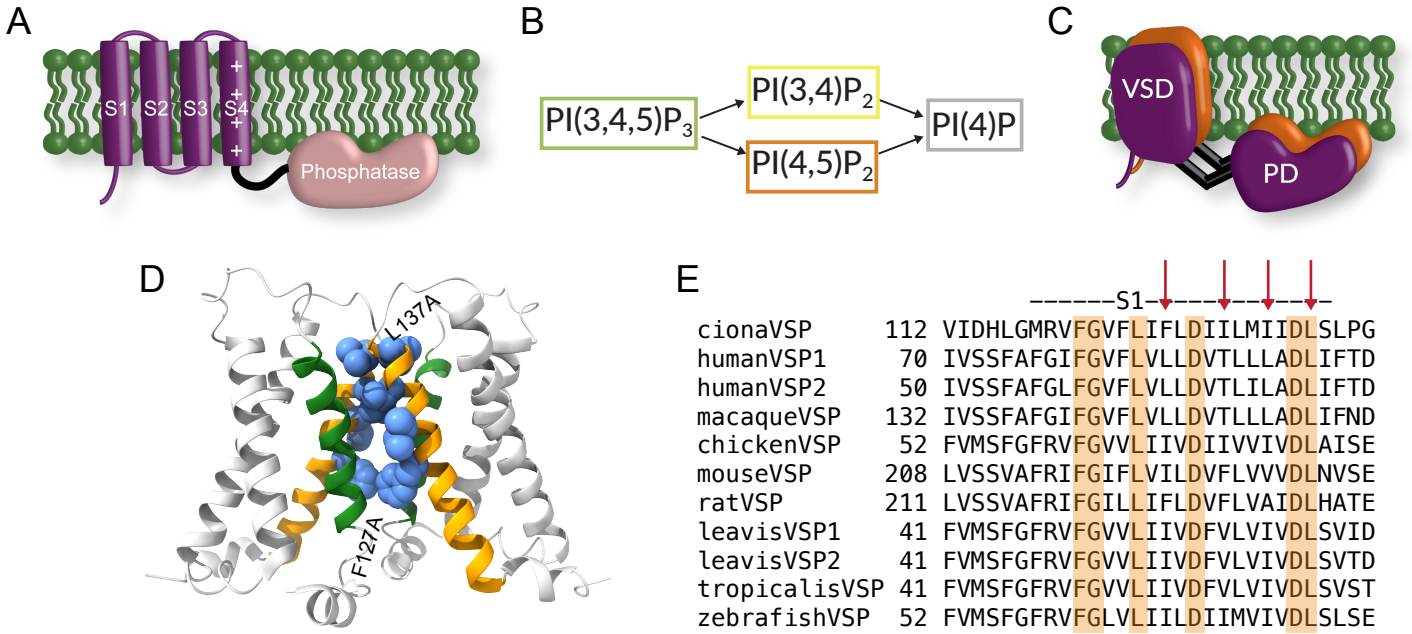

Figure 1: A) Cartoon representation of a single VSP subunit with the four transmembrane helices of the VSD in purple (S1-S4) and the phosphatase domain in peach. B) Reactions catalyzed by VSP. Four different reactions with three different substrates. C) Cartoon representation of a possible VSP dimer organization based on previous results showing both the VSD and phosphatase domains involved in dimerization. D) 4G80 Protein data bank structure of Ci-VSD, biological unit, rendered using ChimeraX (37). The structure suggests a specific dimer interface. Ribbon representation of S1-S4 with S1s in orange and S4s in green. Position F127, I131, I134 and L137 shown in space-filling cartoon. E) Alignment of the VSP S1 helices from several species. Arrows indicate the positions to be mutated to alanine. Sequences for alignments: laevisVSP2, gi|325976472|gb|ADZ48071.1; laevisVSP1, gi|148230800|ref|NP_001090072.1; tropicalisVSP, gi|62859843|ref|NP_001015951.1; macaqueVSP, gi|75076430|sp|Q4R6N0.1; chickenVSP, gi|118084924|ref|XP_417079.2; mouseVSP, gi|76827498|gb|AAI07330.1; ratVSP, gi|157820295|ref|NP_001102347.1; humanVSP2, gi|37788781|gb|AAP45144.1; humanVSP1, gi|213972591|ref|NP_954863.2; zebrafishVSP, gi|70887553|ref|NP_001020629.1; cionaVSP, gi|76253898|ref|NP_001028998.1.

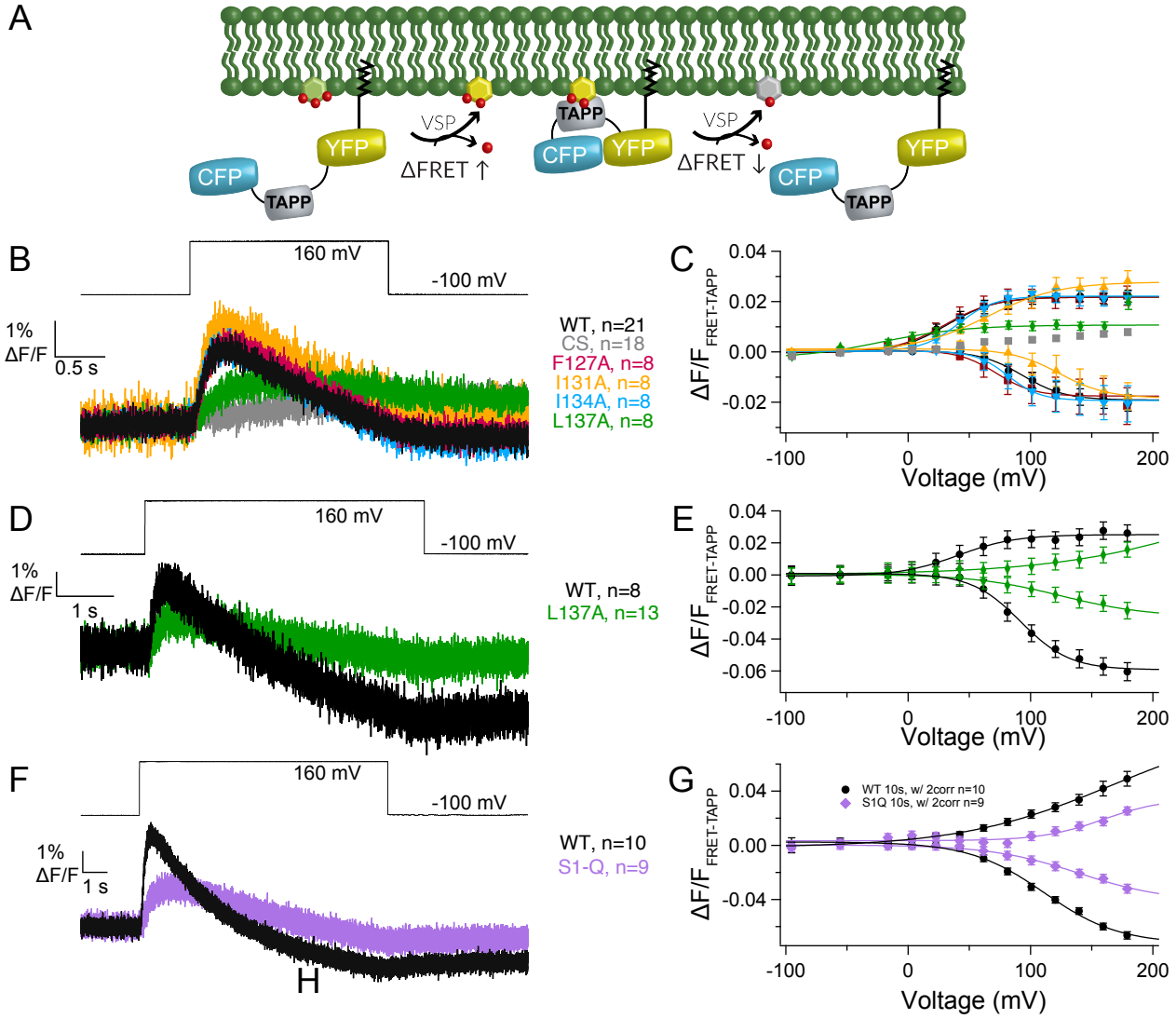

Figure 2: S1 helix modulates kinetics and voltage dependence of PI(3,4,5)P3 and PI(3,4)P2 dephosphorylation. A) Cartoon depicting the biosensor fTAPP's expected response to VSP 5-phosphate dephosphorylation from PI(3,4,5)P3 (increase in FRET) and 3-phosphate dephosphorylation from PI(3,4)P2 (decrease in FRET). B) Averaged fTAPP data for a voltage step from -100 mV holding potential to 160 mV for 2s for the single S1 mutations (F127A, I131A, I134A and L137A). L137A appears to only show 5-phosphatase activity while the others closely resemble WT kinetics of activity. C) Voltage dependent fTAPP activity for the single S1 mutations. The up-FRET component was separated from the down FRET component (see Materials and Methods). While F127A and I134A are very similar to WT, the I131A mutation shifts the voltage dependence of both reactions to higher voltages and the L137A mutation only displays 5-phosphatase activity with the short 2s steps. D) Averaged data for a longer voltage step (5s) from -100 mV to 160 mV for L137A and WT with the CS control subtracted from each (data without subtraction in Supplemental Fig 1B). A clear FRET decrease is visible for L137A at the longer step, indicating that while the mutation does not eliminate 3-phosphatase activity, it slows it down relative to WT. E) L137A voltage dependent fTAPP activity for the 5s voltage step. Both up and down FRET components are visible though the upward component appears more linear. F) Averaged data for a longer voltage step (10s) from -100 mV to 160 mV for S1-Q and WT with the CS control subtracted from each (data without subtraction in Supplemental Fig 1E). A clear FRET decrease is visible for S1-Q at the longer step, indicating that while the mutation does not eliminate 3-phosphatase activity, it slows it down relative to WT. G) S1-Q and WT voltage dependent fTAPP activity for the 10s voltage step. Both up and down FRET components are visible though the upward component appears more linear. All error bars are ± SEM. Data fit with single Boltzmann sigmoid equations.

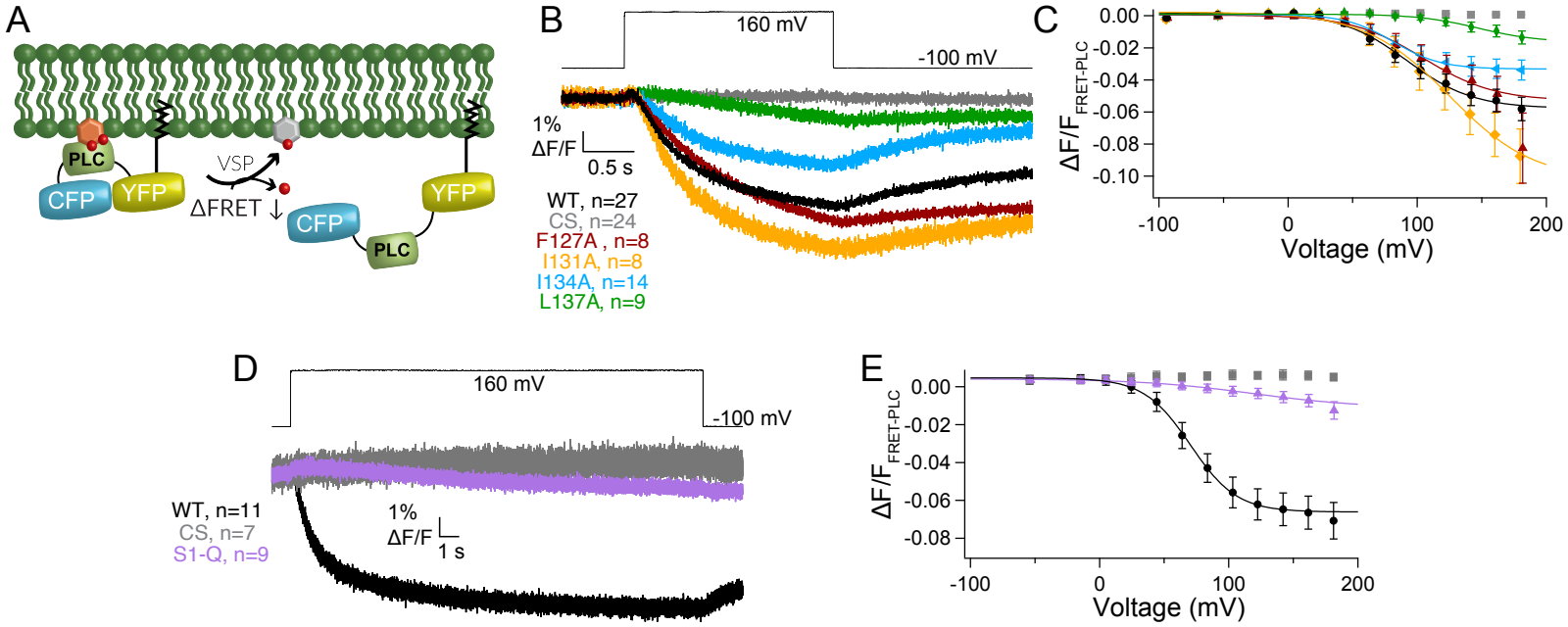

Figure 3: S1 helix impacts kinetics of PI(4,5)P2 5-phosphate dephosphorylation. A) Cartoon depicting the biosensor fPLC's expected response to VSP 5-phosphate dephosphorylation from PI(4,5)P2 (decrease in FRET). B) Averaged fPLC data for a 2s voltage step from -100 mV to 160 mV for the single S1 mutations (F127A, I131A, I134A and L137A). L137A significantly slowed the 5-phosphatase activity while the other mutations more closely resemble WT kinetics. C) Voltage dependent fPLC activity for the single S1 mutations. The I131A mutation shifts the voltage dependence of activity to higher voltages. The L137A mutation displays reduced and right shifted 5-phosphatase activity. D) Averaged data for a long voltage step (20s) from -100 mV to 160 mV for S1-Q and controls. A FRET decrease is visible for S1-Q at the longer step, indicating that while the mutation does not eliminate 5-phosphatase activity, it significantly slows it down. The CS constructs indicates minimal endogenous Xl-VSP2 activity even with such a long pulse. E) Voltage dependent fPLC activity for S1-Q, WT and CS using the longer (20s) pulses. While S1-Q is still active, the activity is almost linear with voltage dependence. All error bars are ± SEM. Data fit with single Boltzmann sigmoid equations.

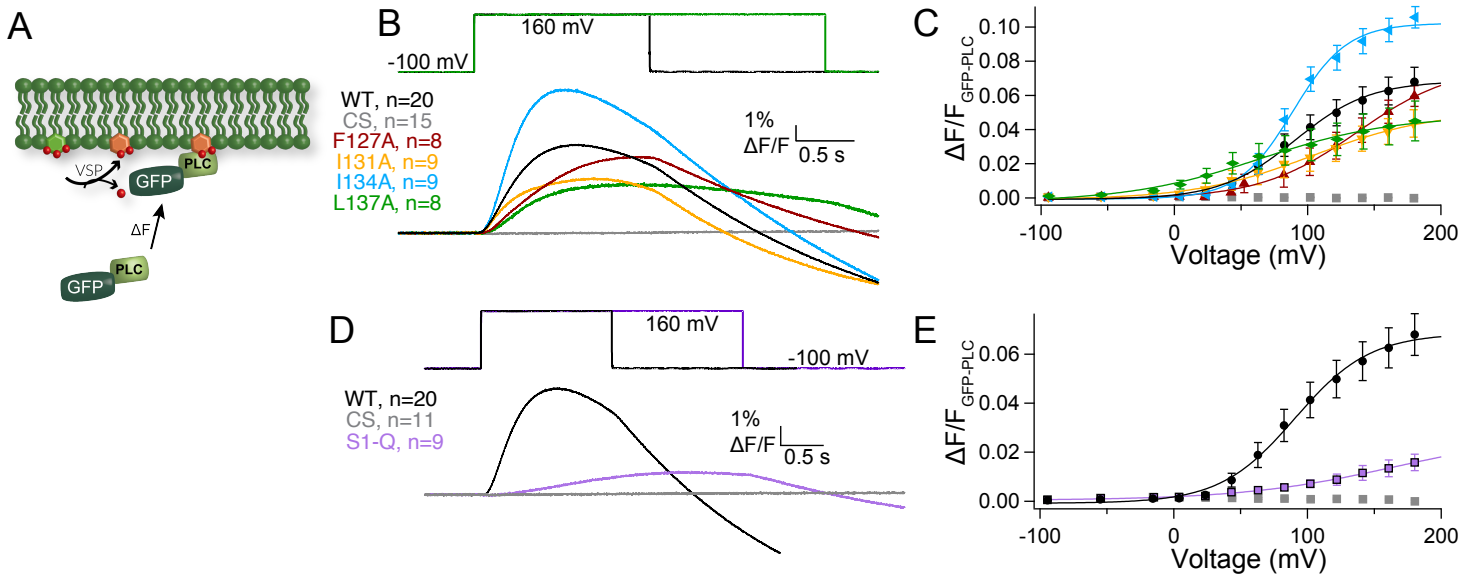

Figure 4: S1 helix modulates the kinetics of PI(3,4,5)P3 3-phosphate dephosphorylation. A) Cartoon depicting the biosensor gPLC's expected response to VSP 3-phosphate dephosphorylation from PI(3,4,5)P3 to PI(4,5)P2 (increased membrane fluorescence). B) Averaged gPLC data for a voltage step from -100 mV to 160 mV for the single S1 mutations (F127A, I131A, I134A and L137A). L137A significantly slowed the 3-phosphatase activity requiring a 3s pulse. C) Voltage dependent gPLC activity for the single S1 mutations. While I134A is similar to WT voltage dependence, it shows an enhanced overall activity. Both the F127A and I131A mutations shift the voltage dependence of activity to higher voltages while L137A displays reduced 3-phosphatase activity and is slightly left shifted though the slope is significantly reduced. D) Averaged data for a voltage step from -100 mV to 160 mV for WT and S1-Q. Slower activation was observed for S1-Q so a 3s pulse was used. E) Voltage dependent gPLC activity for WT and S1-Q. The S1-Q significantly reduced the activity and shifted the voltage dependence to higher voltages, more than just the sum of the individual mutations. All error bars are ± SEM. Data fit with single Boltzmann sigmoid equations.

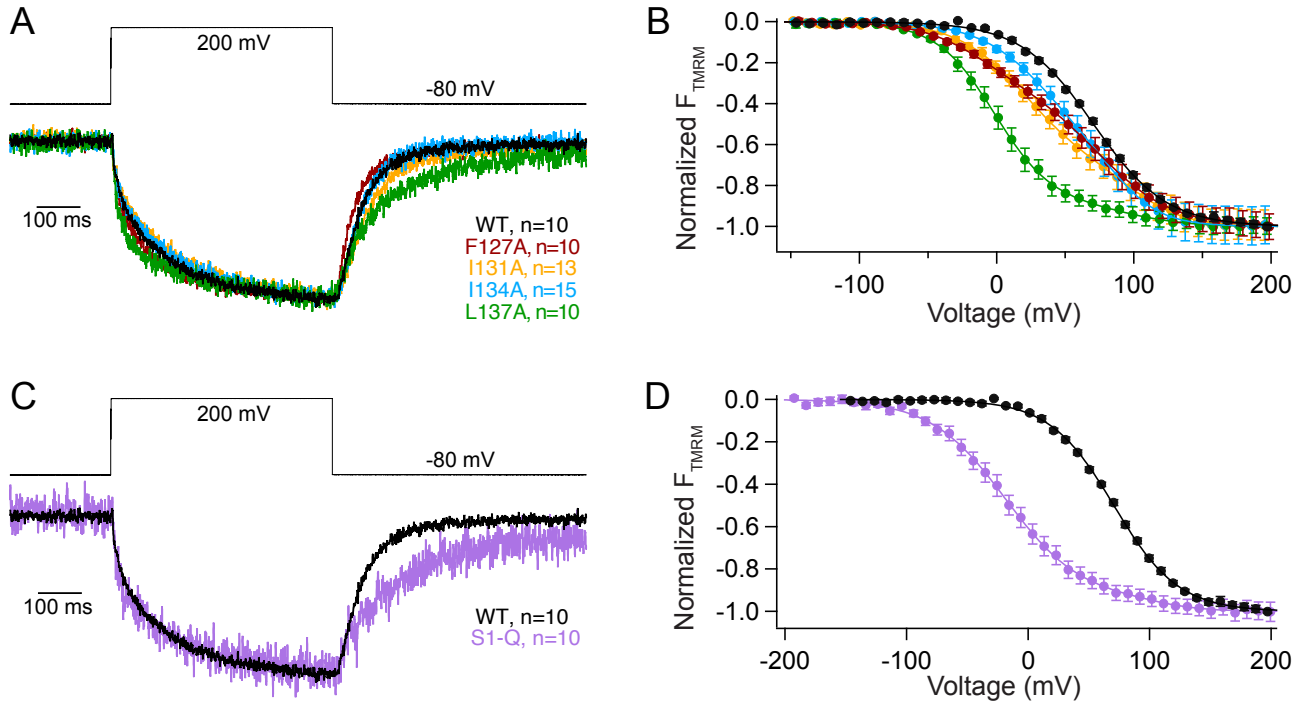

Figure 5: S1 helix tunes voltage dependence of S4 motion. A) Representative VCF traces for a voltage step from -80 mV to 200 mV for all individual S1 mutations. Activation and repolarization kinetics are similar to WT except for L137A which has a second, slower repolarization motion. B) Voltage dependence of the VSD motions. Mutations in S1 of VSP shift the voltage dependence of VSD motions to lower voltages and introduce a second component in the motion. WT fit by single Boltzmann sigmoid while mutants are fit by double Boltzmann sigmoid. C) Representative VCF trace for a voltage step from -80 mV to 200 mV for S1-Q and WT. Repolarization kinetics show an additional slower component for S1-Q. D) The voltage dependent motions of S1-Q significantly shifted the voltage dependence of activation by almost 90 mV compared to WT. It also introduced a second component. WT fit by single Boltzmann sigmoid, and S1-Q fit by double Boltzmann sigmoid. All constructs have an N-terminal His-tag to compare with co-IP data. All errors are ± SEM.

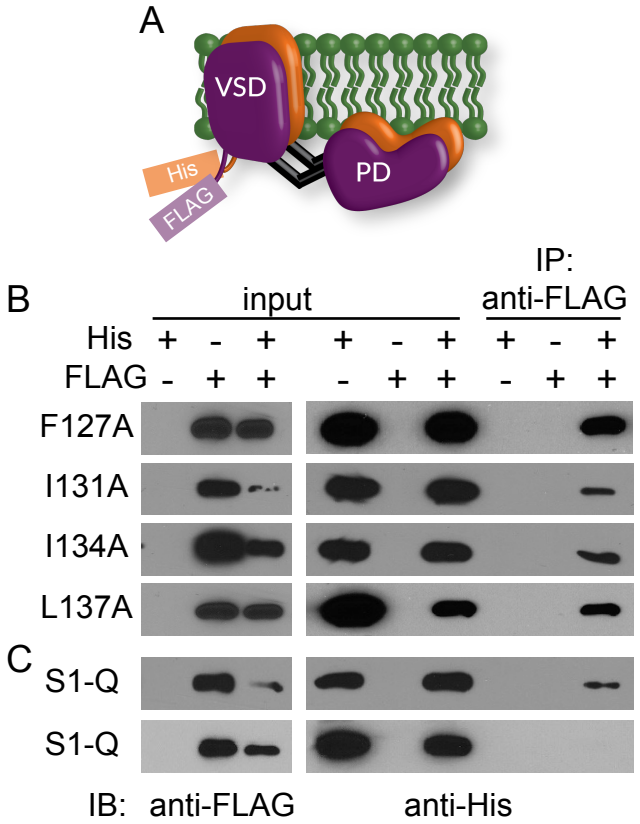

Figure 6. Co-immunoprecipitation pull downs show S1 mutations do not disrupt VSP dimers. A) Cartoon representation of VSP dimers with the His and FLAG tags on the N-terminus. B) Immunoprecipitation assay using individual S1 mutations F127A, I131A, I134A, L137A. Inputs were checked for both FLAG and His to ensure expression. Each blot is representative of at least three pull down blots and shows the FLAG tagged subunit is able to pull down the His-tagged subunit. C) Same experiment with all four mutations on a single subunit, called S1-Q for quad mutation on S1. Top blot shows pull down (representative of four separate experiments) while the bottom blot does not (one blot) even though protein levels are similar between the two.

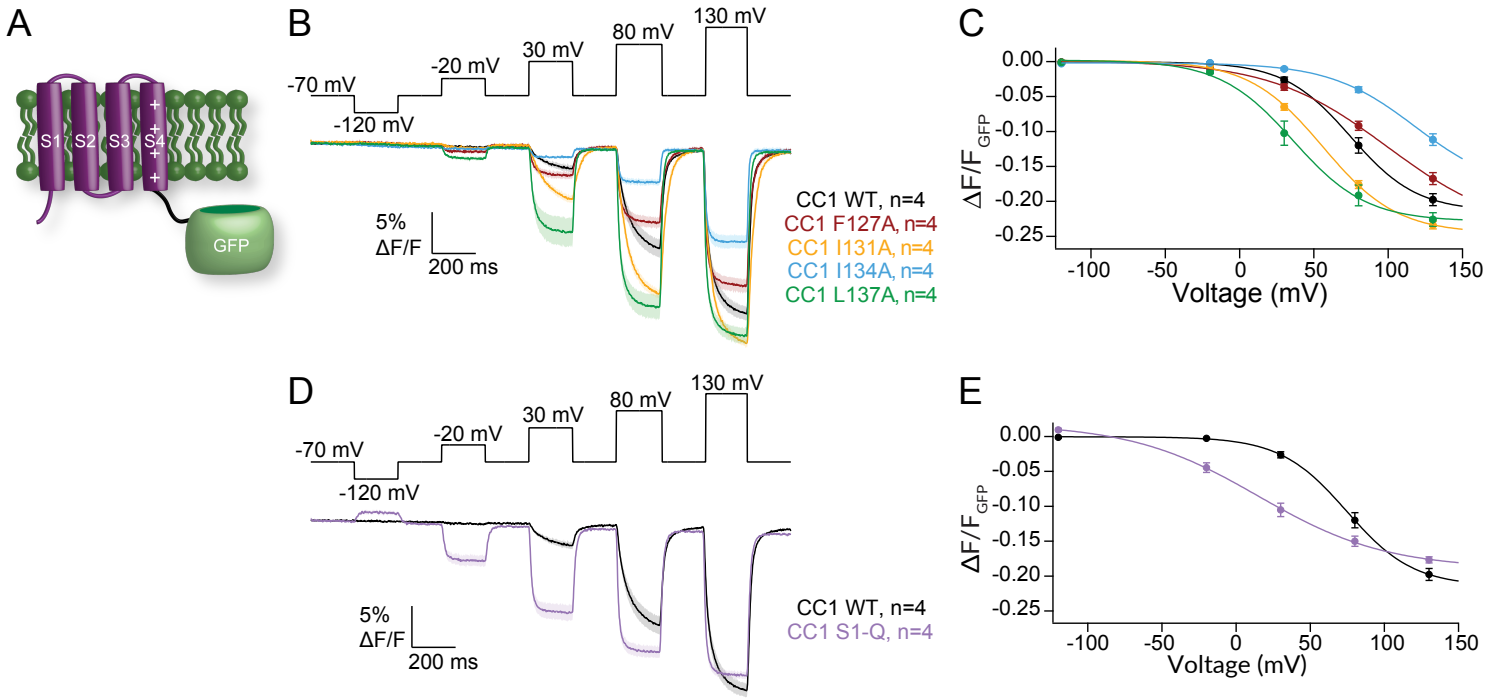

Figure 7: A) Cartoon representation of the GEVI CC1 with the VSD from Ci-VSP attached an FP. B) Averaged series of voltage steps showing kinetics of fluorescence change for CC1 WT and S1 mutants expressed in HEK293 cells. Faster activation and repolarization kinetics observed for F127A, I134A and L137A. C) Voltage dependent fluorescence change for WT and S1 mutations. F127A and I134A shift the voltage dependence to higher voltages while I131A and L137A shift to lower voltages. D) Averaged data for a series of voltage steps for WT and S1-Q. S1-Q shows consistently faster kinetics. E) Voltage dependent fluorescence change for WT and S1-Q. Strong leftward shift consistent with leftward shift from VCF data. All error bars are ± SEM. Data fit with single Boltzmann sigmoid equations.

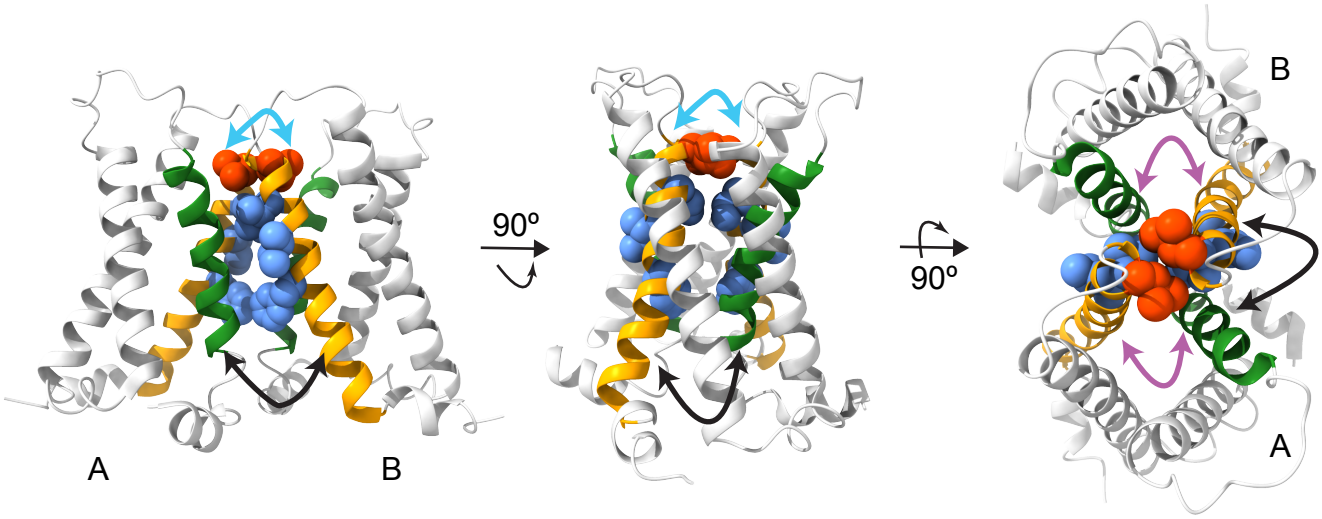

Figure 8. Model for S1 modulation of S4. 4G80 Protein data bank ribbon rendering of Ci-VSD dimers using ChimeraX (37). L137 depicted in red space filling, F127, I131 and I134 depicted in blue space filling, S1 in orange and S4 in green. (left) View is facing into the membrane. S1 from subunit A could be interacting with S4 from subunit B (black arrow) and/or S1 from subunit B (cyan arrow). (middle) Turned in membrane view. Arrows show the same possible interactions. (right) Top-down view shows how the S1 from one subunit can interact with the S4 from the same subunit (purple arrow) as well as the S4 from the adjacent subunit (black arrow). Cyan arrows indicate possible intermolecular interactions through the S1s at the dimer interface between subunits A and B. Black arrows indicate possible intermolecular interactions between the S1 from subunit B to S4 from subunit A. Purple arrows indicate possible intramolecular interactions between the S1 and S4 of the same subunit.